Apéndice

Publicaciones

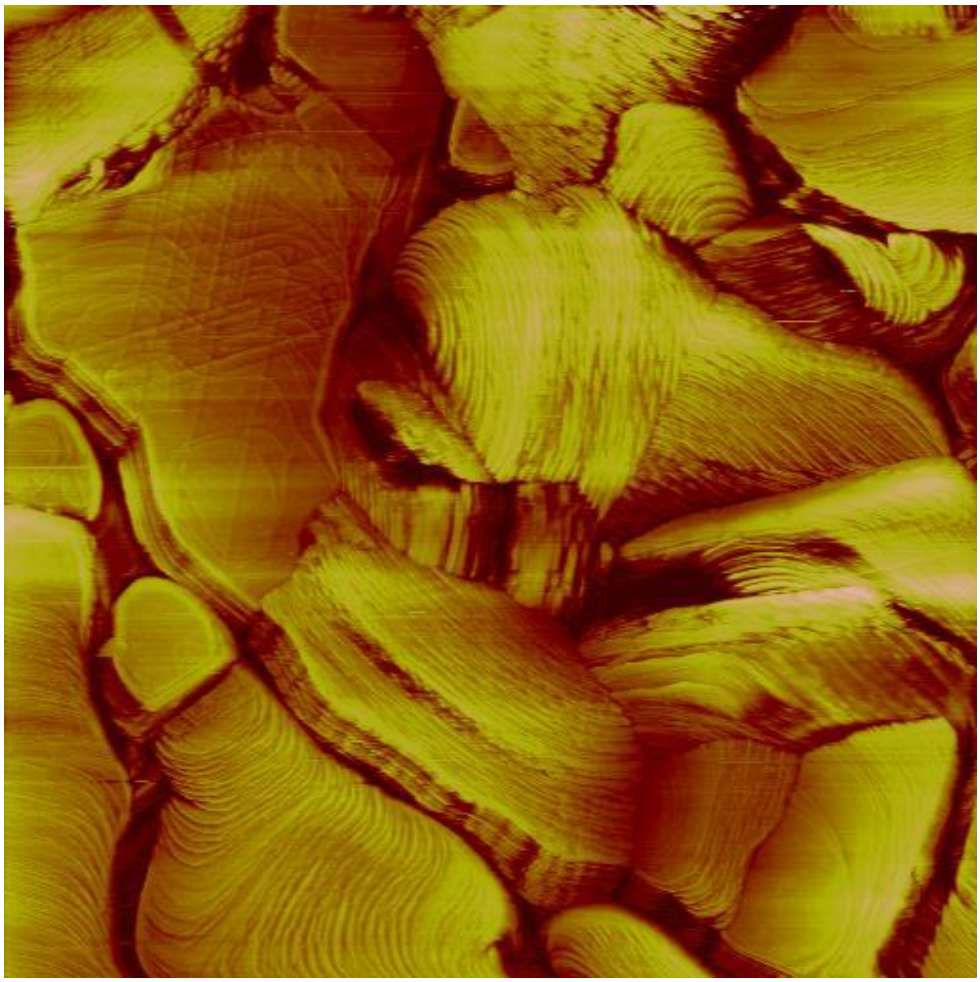

“Fields of gold”

Sting (1993)

Langmuir
Article
pubs.acs.org/Langmuir

Self-Assembly of Alkanedithiols on Au(111) from Solution: Effect of Chain Length and Self-Assembly Conditions

María Antonieta Daza Millone,[†] Hicham Hamoudi,[§,∥] Luis Rodríguez,[‡] Aldo Rubert,[†] Guillermo A. Benítez,[†] María Elena Vela,[†] Roberto C. Salvarezza,[†] J. Esteban Gayone,[‡] Esteban A. Sánchez,[‡] Oscar Grizzi,[‡] Céline Dablemont,[§,∥] and Vladimir A. Esaulov*[,§,∥]

[†]*Instituto de Investigaciones Fisicoquímicas Teóricas y Aplicadas, 1900 La Plata, Buenos Aires, Argentina,* [‡]*Centro Atómico Bariloche, Instituto Balseiro, CNEA, UNCuyo, CONICET, 8400 S.C. de Bariloche, Río Negro, Argentina,* [§]*Université-Paris Sud and* [∥]*CNRS, UMR 8625, Laboratoire des Collisions Atomiques et Moléculaires, LCAM, Bâtiment 351, UPS-11, 91405 Orsay, France*

Received May 5, 2009. Revised Manuscript Received August 24, 2009

A comparative study on the adsorption of buthanedithiol (BDT), hexanedithiol (HDT), and nonanedithiol (NDT) on Au(111) from ethanolic and *n*-hexane solutions and two different preparation procedures is presented. SAM characterization is based on reflection−absorption infrared spectroscopy, electrochemistry, X-ray photoelectron spectroscopy, and time of flight direct recoil spectroscopy. Results indicate that one can obtain a standing-up phase of dithiols and that the amount of the precursor lying-down phase decreases from BDT to NDT, irrespective of the solvent and self-assembly conditions. A good ordering of the hydrocarbon chains in the standing-up configuration is observed for HDT and NDT when the system is prepared in degassed *n*-hexane with all operations carried out in the dark. Disulfide bridges at the free SH terminal groups are formed for HDT and to a lesser extent for NDT prepared in ethanol in the presence of oxygen, but we found no evidence of ordered multilayer formation in our experiments. No disulfides were observed for BDT that only forms the lying-down phase. Our results demonstrate the key role of the chain length and the procedure (solvent nature and oxygen presence) in controlling the surface structure and chemistry of SAMs dithiols on Au(111).

1. Introduction

Dithiols and self-assembled monolayers (SAMs) of these molecules have attracted much attention because of the possibility of using them as linkers between two metallic entities: nanoparticles or metallic surfaces or thin films.[1−5] This is possible because of the availability of two functional SH groups. Numerous reports on the preparation and application of dithiol SAMs are available in the literature. However, in spite of the relatively large amount of work done, the conditions for the reproducible formation of well-ordered SAMs with free SH end-groups have been the object of much debate.[6−12] One of the problems is related to the formation of an initial lying-down phase with the two mercapto groups of the molecule bound to the surface that renders the development of a standing-up phase more complex,[6] than that observed for alkanethiols self-assembly, where only one mercapto group per molecule exists.[13−27] Thus, one could obtain mixed lying-down and standing-up phases.[28,29] The other aspect is related to the possibility of the degradation of the SAMs by

*Corresponding author.

(1) Sarathy, K. V.; Thomas, P. J.; Kulkarni, G. U.; Rao, C. N. R. *J. Phys. Chem. B* **1999**, *103*, 399–401.
(2) Ohgi, T.; Sheng, H. Y.; Nejoh, H. *Appl. Surf. Sci.* **1998**, *130−132*, 919–924.
(3) Sakotsubo, Y.; Ohgi, T.; Fujita, D.; Ootuka, Y. *Physica E* **2005**, *29*, 601–605.
(4) Sakotsubo, Y.; Ohgi, T.; Fujita, D.; Ootuka, Y. *Appl. Surf. Sci.* **2005**, *241*, 33–37.
(5) Ji, H.-F.; Zhang, Y.; Purushotham, V. V.; Kondu, S.; Ramachandran, B.; Thundat, T.; Haynie, D. T. *The Analyst* **2005**, *130*, 1577–1579.
(6) Liang, J.; Rosa, L. G.; Scoles, G. *J. Phys. Chem. C* **2007**, *111*, 17275–17284.
(7) Tai, Y.; Shaporenko, A.; Rong, H. T.; Buck, M.; Eck, W.; Grunze, M.; Zharnikov, M. *J. Phys. Chem. B* **2004**, *108*, 16806–16810.
(8) Niklewski, A.; Azzam, W.; Strunskus, T.; Fischer, R. A.; Woll, C. *Langmuir* **2004**, *20*, 8620–8624.
(9) Yang, Y.-C.; Lee, Y.-L.; Yang, L.-Y. O.; Yau, S.-L. *Langmuir* **2006**, *22*, 5189–5195.
(10) Pasquali, L.; Terzi, F.; Seeber, R.; Doyle, B. P.; Nannarone, S. *J. Chem. Phys.* **2008**, *128*, 134711–10.
(11) Pasquali, L.; Terzi, F.; Zanardi, C.; Pigani, L.; Seeber, R.; Paolicelli, G.; Suturin, S. M.; Mahne, N.; Nannarone, S. *Surf. Sci.* **2007**, *601*, 1419–1427.
(12) Pasquali, L.; Terzi, F.; Zanardi, C.; Seeber, R.; Paolicelli, G.; Mahne, N.; Nannarone, S. *J. Phys.: Condens. Matter* **2007**, *19*, 305020–305020.
(13) Porter, M. D.; Bright, T. B.; Allara, D. L.; Chidsey, C. E. D. *J. Am. Chem. Soc.* **1987**, *109*, 3559–3568.
(14) Nuzzo, R. G.; Fusco, F. A.; Allara, D. L. *J. Am. Chem. Soc.* **1987**, *109*, 2358–2368.
(15) Nuzzo, R. G.; Dubois, L. H.; Allara, D. L. *J. Am. Chem. Soc.* **1990**, *112*, 558–569.
(16) Laibinis, P. E.; Whitesides, G. M.; Allara, D. L.; Tao, Y. T.; Parikh, A. N.; Nuzzo, R. G. *J. Am. Chem. Soc.* **1991**, *113*, 7152–7167.
(17) Hooper, A.; Fisher, G. L.; Konstadinidis, K.; Jung, D.; Nguyen, H.; Opila, R.; Collins, R. W.; Winograd, N.; Allara, D. L. *J. Am. Chem. Soc.* **1999**, *121*, 8052–8064.
(18) Heister, K.; Allara, D. L.; Bahnck, K.; Frey, S.; Zharnikov, M.; Grunze, M. *Langmuir* **1999**, *15*, 5440–5443.
(19) Fisher, G. L.; Hooper, A. E.; Opila, R. L.; Allara, D. L.; Winograd, N. *J. Phys. Chem. B* **2000**, *104*, 3267–3273.
(20) Walker, A. V.; Tighe, T. B.; Cabarcos, O. M.; Reinard, M. D.; Haynie, B. C.; Uppili, S.; Winograd, N.; Allara, D. L. *J. Am. Chem. Soc.* **2004**, *126*, 3954–3963.
(21) Bain, C. D.; Troughton, E. B.; Tao, Y. T.; Evall, J.; Whitesides, G. M.; Nuzzo, R. G. *J. Am. Chem. Soc.* **1989**, *111*, 321–335.
(22) Love, J. C.; Estroff, L. A.; Kriebel, J. K.; Nuzzo, R. G.; Whitesides, G. M. *Chem. Rev.* **2005**, *105*, 1103–1170.
(23) Camillone, N., III; Chidsey, C. E. D.; Liu, G.-y.; Putvinski, T. M.; Scoles, G. *J. Chem. Phys.* **1991**, *94*, 8493–8502.
(24) Camillone, N., III; Chidsey, C. E. D.; Liu, G.-y.; Scoles, G. *J. Chem. Phys.* **1993**, *98*, 3503–3511.
(25) Danisman, M. F.; Casalis, L.; Bracco, G.; Scoles, G. *J. Phys. Chem. B* **2002**, *106*, 11771–11777.
(26) Guo, Z.; Zheng, W.; Hamoudi, H.; Dablemont, C.; Esaulov, V. A.; Bourguignon, B. *Surf. Sci.* **2008**, *602*, 3551–3559.
(27) Prato, M.; Moroni, R.; Bisio, F.; Rolandi, R.; Mattera, L.; Cavalleri, O.; Canepa, M. *J. Phys. Chem. C* **2008**, *112*, 3899–3906.
(28) Kobayashi, K.; Horiuchi, T.; Yamada, H.; Matsushige, K. *Thin Solid Films* **1998**, *331*, 210–215.
(29) Kobayashi, K.; Umemura, J.; Horiuchi, T.; Yamada, H.; Matsushige, K. *Jpn. J. Appl. Phys.* **1998**, *37*, L297–L299.

formation of sulfonates or disulfide bridges and in some cases multilayers, depending upon the type of solvent used[30−34] and preparation procedures. In a recent paper,[35] it was shown using sum frequency generation (SFG), reflection−absorption infrared spectroscopy (RAIRS), and spectroscopic ellipsometry that well-ordered SAMs of standing-up nonanedithiol (NDT) could be produced in *n*-hexane provided that N_2-degassed solutions are used and all preparation steps are performed in the absence of ambient light. It was, in particular, observed that exposure to light in ambient conditions led to an attenuation of the SH signal.

In case of alkanethiol self-assembly, it is generally considered[16] that the degree of order in the SAM improves with increasing chain length. In this respect, one can ask oneself whether the quality of a dithiol SAM would worsen with short chain lengths. Many applications in nanotechnology and nanoscience, which requires charge transfer using dithiols as bridges, would be optimized using short molecules in the standing-up configuration. However, in a recent paper it was reported that the shorter hexanedithiol (HDT) only forms an ordered array of lying-down molecules in both gas-phase and liquid environments.[36] On the other hand, standing-up multilayer formation by spontaneous organization of HDT on Au has been reported by other authors.[30] The linking chemistry between layers was proposed to be the oxidative formation of a sulfur−sulfur bond that competes successfully with intralayer S−S bond formation. Therefore, the behavior of HDT molecules on the Au(111) phase deserves particular attention concerning not only the surface structure, but also the SAM chemistry and quality.

In this work, we investigate the HDT adsorption on Au(111) from the liquid phase using two different solvents (*n*-hexane and ethanol) following different procedures described previously in the literature.[35] The results are compared to those obtained for butanedithiol (BDT) and NDT SAMs prepared under the same experimental conditions. A multitechnique approach involving electrochemistry, X-ray photoelectron spectroscopy (XPS), reflection−absorption infrared spectroscopy (RAIRS), and time-of-flight direct recoil spectroscopy (TOF-DRS) is used to analyze the SAMs. The latter combines the ability to detect all elements, including H, which are not detected in most electron spectroscopies, with a very high surface sensitivity (topmost layers) and very low irradiation dose (picoampere currents), thus preventing significant damage of the film. We have used this technique successfully to investigate the adsorption/desorption kinetics of some alkanethiol SAMs.[37−39]

It is found in both solvents that the amount of the lying-down phase decreases sharply from BDT to NDT. In contrast to previous results,[36] which only reported the existence of the lying-down phase, we observe dominant formation of the standing phase in HDT SAMs in both solvents. A good ordering of the hydrocarbon chains in the standing-up configuration is observed for NDT when the system is prepared in degassed *n*-hexane with all operations carried out in the dark. Disulfide bridges at the free SH terminal groups are formed for HDT and to a lesser extend for NDT prepared in ethanol, but we found no evidence of ordered multilayer formation[30] in our experiments. No disulfides were observed for BDT that only forms the lying-down phase. Our results demonstrate the key role of the chain length and the self-assembly procedure (solvent nature and oxygen presence) in controlling the surface structure and chemistry of SAMs dithiols on Au(111). We also found that *n*-hexane is a promising solvent for the formation of densely packed, well-ordered SAMs when they are prepared in absence of oxygen and light.

2. Experimental Section

2.1. Gold Substrates. In order to get well-organized SAMs, the quality of the gold surface is a key parameter. Here, we used gold on glass substrates and a gold monocrystal.

The Au(111) sample was obtained from MaTecK GmbH as a single crystal hat-shaped disk (10 mm diameter, 3 mm thick, hat shape with the usable sample face of 8 mm diameter) of 99.999% purity, oriented to within $<0.4°$. The surface geometry was checked by both LEED and TOF-DRS. In order to reduce the strong effect that surface roughness or contamination may have on the adsorption kinetics, particular care was taken to clean in situ in the high-vacuum chamber the initial crystalline Au surface by cycles of Ar sputtering and annealing to 500 °C.

The gold on glass substrates were made of 0.7-mm-thick borosilicate glass, covered by a 2.5-nm-thick chromium adhesion layer, and by a 250-nm-thick final gold layer. For this work, the substrates were annealed with a H_2 flame during 3 min or in a furnace to 600 °C in order to produce flat terraces with (111) preferred orientation.

It should be noted here that, while in a given laboratory systematically similar preparation conditions are used, morphological differences in samples may exist regarding size of flat domains and small terraces especially on gold on mica substrates. Since RAIRS and TOF-DRS involve grazing scattering conditions, they "see" the top flat terraces as opposed to electrochemistry and XPS, where a fuller picture of the sample is obtained. Since the assembly characteristics on terraces and elsewhere may not be the same, this could affect conclusions from the different techniques. However, the data we present draws a complementary consistent picture.

2.2. Chemicals. 1,4-Butanedithiol (BDT), 1,9-nonanedithiol (NDT) 97%, and 1,6-hexanedithiol (HDT) 97% were purchased from Alfa Aesar and Sigma and *n*-hexane 99% from Riedel-de Haën. Some comparative measurements were performed on some alkanethiols. 1-Propanethiol (PT) 99%, 1-butanethiol (BT) 99%, 1-hexanethiol (HT) 95%, 1-nonanethiol (NT) 95%, and 1-decanethiol (DT) 96% were purchased from Sigma and Fluka. All chemicals were used without further purification. All other chemicals were of best analytical grade available.

2.3. SAMs Preparation. Alkanethiol SAMs were prepared by immersing the gold support into a freshly prepared 50 μM or 1 mM solution of C_nSH in ethanol for times ranging from 30 min to 24 h at room temperature in the absence of light. Final rinsing was done with absolute ethanol before drying under N_2. These measurements were done as a reference for the dithiol SAMs.

In the case of alkanedithiols, SAMs were prepared by two methods. In the first one (procedure I), the Au substrates were immersed in 50 μM dithiol solution in ethanol for 24 h, i.e., following the usual protocol for alkanethiol SAM formation but in the absence of light. In the second one (procedure II), the SAMs were prepared by immersing the Au substrates into a 1 mM

(30) Kohli, P.; Taylor, K. K.; Harris, J. J.; Blanchard, G. J. *J. Am. Chem. Soc.* **1998**, *120*, 11962–11968.
(31) Carot, M. L.; Esplandiu, M. J.; Cometto, F. P.; Patrito, E. M.; Macagno, V. A. *J. Electroanal. Chem.* **2005**, *579*, 13–23.
(32) Käshammer, J.; Wohlfart, P.; Weiss, J.; Winter, C.; Fischer, R.; Mittler-Neher, S. *Opt. Mater.* **1998**, *9*, 406–410.
(33) Esplandiu, M. J.; Carot, M. L.; Cometto, F. P.; Macagno, V. A.; Patrito, E. M. *Surf. Sci.* **2006**, *600*, 155–172.
(34) Rieley, H.; Kendall, G. K.; Zemicael, F. W.; Smith, T. L.; Yang, S. *Langmuir* **1998**, *14*, 5147–5153.
(35) Hamoudi, H.; Guo, Z.; Prato, M.; Dablemont, C.; Zheng, W. Q.; Bourguignon, B.; Canepa, M.; Esaulov, V. A. *PhysChemChemPhys* **2008**, *10*, 6836–6841.
(36) Leung, T. Y. B.; Gerstenberg, M. C.; Lavrich, D. J.; Scoles, G.; Schreiber, F.; Poirier, G. E. *Langmuir* **2000**, *16*, 549–561.
(37) Rodríguez, L. M.; Gayone, J. E.; Martiarena, M. L.; Sánchez, E. A.; Grizzi, O.; Blum, B.; Salvarezza, R. C.; Xi, L.; Lau, W. M. *Nucl. Instrum. Methods Phys. Res., Sect. B* **2007**, *258*, 183–188.
(38) Rodríguez, L. M.; Gayone, J. E.; Sánchez, E. A.; Grizzi, O.; Blum, B.; Salvarezza, R. C. *J. Phys. Chem. B* **2006**, *110*, 7095–7097.
(39) Rodríguez, L. M.; Gayone, J. E.; Sánchez, E. A.; Grizzi, O.; Blum, B.; Salvarezza, R. C.; Xi, L.; Lau, W. M. *J. Am. Chem. Soc.* **2007**, *129*, 7807–7813.

solution in *n*-hexane for about 1 h with N_2 bubbling. In this case, we used solutions freshly degassed by N_2 bubbling, and all procedures were carried out in the absence of light. In the case of the volatile hexane, in order to avoid solvent evaporation and consequently a concentration increase in Orsay, hexane was first bubbled with N_2, then the dithiol was added, and after introduction of the sample, the solution was kept sealed off. In La Plata, N_2 bubbling was maintained during substrate modification, which was performed under a hood in a glass device with a reflux system. It should be noted that *n*-hexane vapors can be explosive and they have toxic effects when inhaled. It is therefore recommended to use appropriate precautions and perform all operations under a hood.

2.4. Electrochemical Measurements. Standard three-electrode electrochemical cells were employed with an operational amplifier potentiostat (TEQ-Argentina) with data acquisition capabilities. A saturated calomel electrode (SCE) and a large area platinum foil were used as reference and counter electrode, respectively. All potentials in the text are referred to the SCE scale. The base electrolyte, 0.1 M NaOH aqueous solution, was prepared with Milli-Q water and solid NaOH (analytical grade from Baker) and was degassed with purified nitrogen prior to the experiments. Reductive electrodesorption of thiols from the Au substrates was performed at 0.05 V s^{-1} in deaerated aqueous 0.1 M NaOH at room temperature.

2.5. XPS Measurements. The samples were characterized by XPS using a Mg Kα source (XR50, Specs GmbH) and a hemispherical electron energy analyzer (PHOIBOS 100, Specs GmbH). A two-point calibration of the energy scale was performed using sputtered cleaned gold (Au $4f^{7/2}$, binding energy (BE) = 84.00 eV) and copper (Cu $2p^{3/2}$, BE = 933.67 eV) samples. For spectra deconvolution of the S 2p region, a Shirley-type background was subtracted and a combination of Lorenzian and Gaussian (Voigt) functions was used. The full width at half-maximum (fwhm) was fixed at 1.1 eV and the spin−orbit doublet separation of S 2p signal was set to 1.2 eV. The BEs and peak areas were optimized to achieve the best adjustment.

Sulfur coverage was estimated by the measurement of the areas of Au 4f and S 2p signals corrected by the relative sensitivity factor (RSF) of the elements. Au 4f signal was corrected by the attenuation length for electrons in Au to consider only the signal of the top Au atomic monolayer. Therefore, sulfur coverage is the ratio of sulfur atoms to Au atoms on the surface, taking into account every chemical form of sulfur.

2.6. Infrared Spectroscopy. As in our previous work in Orsay the FT-IR spectrometer used for analysis is a Bruker Vertex 70, equipped with a homemade reflection attachment for RAIRS measurements. In this case, the incident angle was 80° to the surface normal. A deuterated triglycine sulfate (DTGS) detector was used to detect either the transmitted or reflected light. For the SAM measurements, the spectral resolution was set to 4 cm^{-1}. The spectrometer and sample are flushed first with dry air and during measurements by a N_2 flow.

2.7. Time of Flight Spectroscopy. The measurements were carried out on a UHV apparatus equipped for the atomic and electronic spectroscopies (TOF-DRS, AES, and UPS). The UHV chamber is connected to a 1−100 keV ion accelerator through three stages of differential pumping. Details of the experimental setup and the TOF-DRS technique have been described previously.[40]

Briefly, the method consists of bombarding the sample at grazing incidence with a pulsed Ar ion beam. The time-of-flight spectrum of directly recoiled ("sputtered") fast atoms is measured and allows determination of their mass spectrum. This method combines the ability to detect all elements, including H, which is not detected in most electron spectroscopies, with a very high surface sensitivity (topmost layers) and very low irradiation dose (picoampere currents), thus preventing significant damage of the film. We have used this technique successfully to investigate the adsorption/desorption kinetics of some alkanethiol SAMs.[37−39]

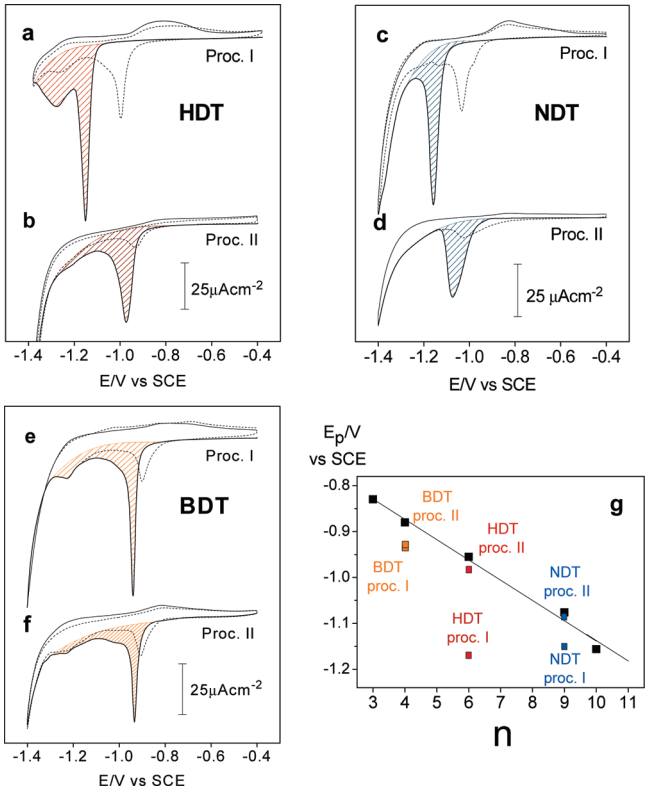

Figure 1. *j* vs *E* profiles for the reductive desorption of HDT (a,b), NDT (c,d), and BDT (e,f) SAMs from Au (111). Self-assembly conditions were 24 h, 50 μM ethanolic solution in air (a,c,e), and 1 h 1 mM *n*-hexane deoxygenated solution (b,d,f). First scans are in full line and second scans in dashed lines. Integration areas for charge calculation are represented in dashed red, blue, and orange. Measurements were made in 0.1 M NaOH at a sweep rate of 0.05 V s^{-1} g) E_p vs *n* (*n*: number of C atoms) plot derived from reductive polarization curves for alkanethiolates (black squares), BDT (orange squares), HDT (red squares), and NDT (blue squares).

The ions (Ar^+), used for sample cleaning and for the TOF-DRS measurements, were produced in a radiofrequency source, mass analyzed with a switching magnet, and finally collimated to better than 0.1°. For TOF-DRS, the Ar beam was pulsed at 30 kHz, with 50 ns width. The system allowed TOF measurements as a continuous function of the scattering angle (within the range of 0° to 70°) by using a rotatable drift tube of 75 cm and also at some fixed scattering angles with a longer flight path for the scattered particles (176 cm for a 30° TOF tube).

3. Results

3.1. Electrochemical Measurements. *3.1.1. BDT, HDT, and NDT Prepared by Procedure I.* Figure 1a,c,e shows typical cathodic current density (*j*)/potential (*E*) curves (first and second scans) recorded in a 0.1 M NaOH aqueous solution for the different dithiol SAMs prepared by procedure I. The cathodic current peaks preceding the current related to the hydrogen evolution reaction (HER) are assigned to the reductive desorption of dithiols from the Au substrates.[41]

In Figure 1a, a typical desorption curve recorded for a HDT SAM prepared by this procedure is depicted. The first scan shows

(40) Rodríguez, L. M.; Gayone, J. E.; Sánchez, E. A.; Ascolani, H.; Grizzi, O.; Sánchez, M.; Blum, B.; Benitez, G.; Salvarezza, R. C. *Surf. Sci.* **2006**, *600*, 2305–2316.

(41) Vela, M. E.; Martin, H.; Vericat, C.; Andreasen, G.; Hernandez Creus, A.; Salvarezza, R. C. *J. Phys. Chem. B* **2000**, *104*, 11878–11882.

a well-defined peak located at −1.14 V followed by a broad and poorly defined peak preceding HER. The overall charge density (q), measured by integration of these current peaks referred to the real surface area, yields 130 ± 3 μC cm^{-2}, a result that exceeds by ~60% the expected amount for a complete HDT monolayer in standing-up configuration (surface coverage 1/3, q = 75 μC cm^{-2}[41]).

For alkanethiols, we have found that the peak potential E_p varies linearly with the length of the alkane chain as shown in Figure 1g. Here, we observed a marked shift in the peak potential (E_p) of the HDT SAM to more negative values (about 0.150 V) with respect to that measured for a hexanethiol (HT) SAM prepared by using the same procedure and substrate (Figure 1g). Significant readsorption of the organic products takes place during repetitive potential scans. The reductive desorption of the readsorbed species (dashed curve in Figure 1a) takes place at −0.97 V, i.e., 0.15 V more positive than that recorded for the first scan and close to the potential corresponding to the HT. These results for the HDT SAMs prepared in ethanol are in good agreement with previous reports for this system.[42]

Similar results to those described for HDT were obtained for NDT prepared by the same procedure (Figure 1c). In fact, for the NDT sample prepared in ethanol we also observed an important E_p shift in the negative direction (0.07 V) with respect to nonanethiol (NT) (Figure 1g) and also significant readsorption in the second scan. However, in this case the q value, 81 ± 6 μC cm^{-2}, is smaller than that observed for HDT and close to the expected value for a dense monolayer of dithiols in standing-up configuration.

On the other hand, for BDT we observe a negative shift in E_p of 0.06 V with respect to butanethiol SAM on Au (111). In this case, the q value is also found to be 79 ± 10 μC cm^{-2}. However, for the short BDT the same amount of thiolates is expected for the lying-down and standing-up configurations. In fact, in both cases it is possible to arrange the thiolates in $\sqrt{3} \times \sqrt{3}$ $R30°$ lattice. Therefore, from the electrochemical data we cannot conclude the possible configuration of the BDT molecules. Also, no significant readsorption was observed during repetitive scans (Figure 1e).

In summary, electrochemical data suggest that for HDT and NDT prepared by procedure I the molecules are mostly in standing-up configuration but the free SH groups has been altered by chemical reactions at the outer plane of the SAMs, in agreement with previous works.[33,42] In the case of BDT, we cannot conclude from the electrochemical experiments whether the molecules are in lying-down or standing-up configuration; this will be clarified by XPS data as discussed below.

3.1.2. BDT, HDT, and NDT Prepared by Procedure II. In Figure 1b, we show the j/E profiles recorded for HDT SAMs on Au(111) prepared by procedure II, i.e., in a degassed n-hexane solution in the absence of light. In this case, a well-defined peak related to reductive desorption is observed at −0.97 V followed by a small shoulder preceding HER. The q value is 81 ± 4 μC cm^{-2}, a figure very close to that expected for an HDT monolayer in a standing-up configuration.[43] The E_p value is shifted only 0.02 V in the negative direction when compared with the HT SAM on Au (Figure 1g). As we observed for electrodesorbed alkanethiolates,[44] no significant readsorption was detected during repetitive electrode cycling.

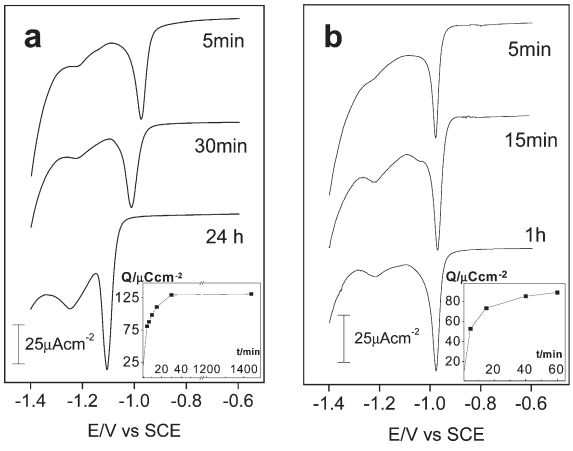

Figure 2. j vs E profiles for the reductive desorption of HDT SAMs from Au (111) for different immersion time. Self-assembly conditions were (a) HDT 50 μM ethanolic solution in air and (b) HDT 1 mM n-hexane deoxygenated solution. Insets show q vs t plots for each case. Measurements were made in NaOH 0.1 M at a sweep rate of 0.05 V s^{-1}.

On the other hand, for NDT SAMs (Figure 1b) we found a smaller q value (q = 60 ± 5 μC cm^{-2}) than that measured for HDT, and also a negligible E_p shift with respect to the corresponding alkanethiolate (Figure 1g).

Finally, for BDT SAMs (Figure 1f) the same results described for the self-assembly of this dithiol by procedure I were observed (Figure 1e). In fact, we found a negative shift in E_p = 0.05 V with respect to butanethiolate on Au(111) and no significant readsorption, although q is slightly smaller (q = 70 ± 10 μC cm^{-2}) than that observed for BDT prepared by procedure I.

The main conclusion for dithiol self-assembly by procedure II is that no clear evidence about chemical transformation of the terminal SH groups can be found in the electrochemical experiments.

3.1.3. Immersion Time Dependence of the HDT Reductive Desorption Curves. In Figure 2a, we have plotted electrodesorption curves for Au surfaces immersed for different times (t_i) in 50 μM HDT ethanolic solutions following procedure I. It is evident that as t_i is increased E_p shifts from −0.97 V to −1.105 V while q increases from 55 μC cm^{-2} to 130 μC cm^{-2}. On the other hand, in similar experiments made in n-hexane solutions by procedure II (Figure 2b), no shift in E_p is observed and the increase in q is from 53 μC cm^{-2} to 80 μC cm^{-2}.

The smaller values in both solvents observed at shorter times, are consistent with what is expected in the model presented in ref 36 for HDT in lying-down configuration. The second value, mentioned above, in the case of n-hexane agrees with that expected for a close-packed $\sqrt{3} \times \sqrt{3}$ $R30°$ HDT lattice (surface coverage θ_{DS} = 1/3) with the molecules in the vertical configuration,[43] while for HDT adsorption from the ethanolic solution q largely exceeds this value.

These results for HDT suggest that irrespective of the self-assembly procedure the molecules first arrange in lying-down configuration and then rearrange into a dense dithiol layer consisting mainly of molecules in standing-up configuration. In the ethanol solution, the standing-up HDT phase is formed more rapidly (less than 10 min; the time needed to attain 80 μC cm^{-2}) than in n-hexane (40 min) despite the higher HDT concentration in this solvent. However, for t > 10 min the SAM formed in ethanol is transformed into a structure containing an excess of

(42) Esplandiu, M. J.; Hagenstrom, H.; Kolb, D. M. *Langmuir* **2001**, *17*, 828–838.
(43) Vericat, C.; Vela, M. E.; Salvarezza, R. C. *PhysChemChemPhys* **2005**, *7*, 3258–3268.
(44) Terán Arce, F.; Vela, M. E.; Salvarezza, R. C.; Arvia, A. J. *Langmuir* **1998**, *14*, 7203–7212.

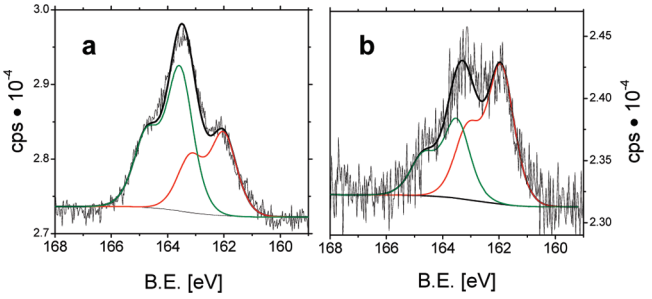

Figure 3. S 2p XPS spectra of HDT SAMs (a) SAMs obtained after 24 h incubation in 50 μM ethanolic solution (procedure I), (b) SAMs obtained after 1 h incubation in 1 mM *n*-hexane solution (procedure II). Red: 162 eV component. Green: 163.5 eV component.

S-containing organic products. Therefore, in order to analyze the nature of the S-containing molecules on the Au (111) surface XPS measurements were made.

3.2. XPS Data. *3.2.1. HDT SAMs from Procedure I.* The XPS S 2p spectra for the HDT SAMs on Au (111) prepared by procedure I are shown in Figure 3a. The broad S 2p signal, typical of metals covered by SAMs, can be fitted with two doublet components located at 162.0 and 163.5 eV. The first component (162 eV) corresponds to thiolates adsorbed on metals, while the component at 163.5 eV can be assigned to free thiol (SH) groups or disulfides.[45]

The coverages of the standing-up and lying-down phases were evaluated in two different ways depending upon the S 2p (163.5 eV)/S 2p (162 eV) ratio.

(i) If the ratio of the S 2p signal at 163.5 eV with respect to 162 eV was higher than that expected for all the molecules in the standing-up position, we calculate the coverage of standing-up molecules from the ratio S 2p (162 eV)/Au 4f (84 eV) and assign the excess of S 2p (163 eV) to free dithiols or disulfides.

(ii) If the S 2p (163.5 eV)/S 2p (162 eV) ratio was lower than that expected for the all standing-up configuration, then we calculate the standing-up phase coverage from the signal of S 2p at 163.5 eV and the excess of S 2p (162 eV) was assigned to lying-down dithiol molecules.

By using these rules, the total coverage by dithiol molecules for the HDT SAM formed in ethanol by procedure I is found to be $\theta_{DS} = 0.41 \pm 0.03$, exceeding by 24% that expected for a complete monolayer of HDT in the standing-up configuration ($\theta_{DS} = 0.33$) formed on Au (111).[43] The amount of thiolates calculated from the signal at 162 eV coincides with that expected for a monolayer of thiolates in vertical configuration forming a $\sqrt{3} \times \sqrt{3}$ $R30°$ surface structure prepared by the same self-assembly procedure.[46,47] Therefore, the excess of molecules is related to the 163.5 eV component. In principle, this signal should be assigned to free HDT molecules or disulfide species. However, repetitive rinsing with pure solvent does not reduce the intensity of the 163.5 eV signal, so we conclude that we do not have any physisorbed dithiols in the SAM. Therefore, the 163.5 eV signal contains the contribution of *extra* HDT molecules bonded to the terminal group of the thiolate SAM by S−S bonds. The presence of

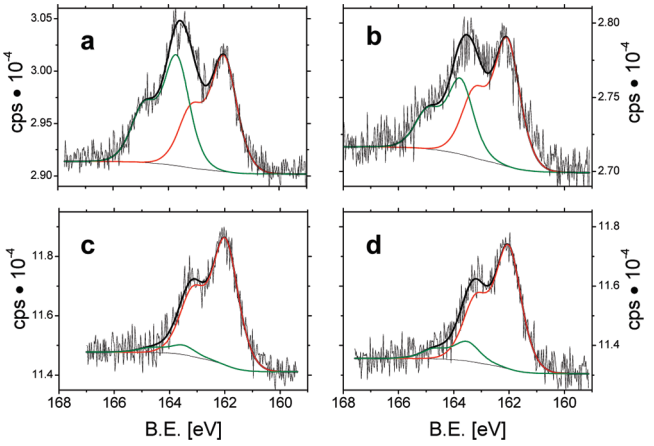

Figure 4. S 2p XPS spectra of NDT SAMs. (a) SAMs obtained after 24 h incubation in 50 μM ethanolic solution (procedure I), (b) SAMs obtained after 1 h immersion in 1 mM *n*-hexane solution (procedure II). S 2p XPS spectra of BDT SAMs (c) SAMs obtained by procedure I, (d) SAMs obtained by procedure II. Red: 162 eV component. Green: 163.5 eV component.

disulfide bonds is also supported by the extra charge needed in the reductive desorption experiments (section 3.1, Figures 1a and 2a). In fact, it is well-known that electrolytic cleavage of disulfide bonds at a mercury pool cathode can be used to measure the total amount of disulfide bonds in proteins.[48]

Therefore, these results suggest that HDT SAMs prepared by procedure I form a complex adlayer consisting of a monolayer of HDT molecules bonded to the gold substrate by thiolates ($\theta_{DS} = 0.33$), and also HDT molecules bonded by disulfide S−S bonds at the SAM surface and/or extra HDT molecules strongly bonded to the terminal group of the layer by S−S bonds ($\theta_{DS} = 0.08 \pm 0.03$). The latter explain the larger 163.5 eV signal in XPS.

It should be mentioned that in our series of measurements the HDT samples in ethanol only occasionally exhibit the presence of sulfonates (167 eV) due to the oxidation of the ourtermost S moiety, at least for 24 h of incubation in this solvent.[49]

3.2.2. HDT SAMs from Procedure II. XPS data obtained for HDT SAMs prepared by procedure II are shown in Figure 3b. Also, in these samples we observe the 162.0 eV (thiolates) and 163.5 eV components. The coverage by dithiol molecules estimated by the S/Au ratio is $\theta_{DS} \approx 0.23 \pm 0.03$, a figure smaller than that expected for close-packed HDT SAM with molecules in a vertical configuration. The analysis of the two components (162/163.5 eV ratio) indicates that there is an excess of the 162 eV signal (thiolates) with respect to that expected for a standing-up monolayer of HDT. The excess of thiolates and the smaller value of θ_{DS} suggests that the HDT SAM contains some mixed domains of standing-up and lying-down molecules. Considering the excess of thiolates (from the 162/163.5 signal ratio), we estimate a surface coverage $\theta_{DS} = 0.15 \pm 0.04$ for the standing-up phase and $\theta_{DS} = 0.08 \pm 0.04$ for the lying-down phase. The 163.5 eV component can be assigned to the free SH terminal group of the molecules in standing-up configuration based on the electrochemical data that show no evidence of extra-charge and E_p shift during the reductive desorption.

3.2.3. BDT and NDT SAMs. XPS spectra for NDT and BDT are shown in Figure 4. In the case of NDT, both procedures lead to θ_{DS} values slightly smaller than that expected for a full

(45) Lindberg, B. J.; Hamrin, K.; Johansson, G.; Gelius, U.; Fahlman, A.; Nordling, C.; Siegbahn, K. *Phys. Scr.* **1970**, *1*, 286–298.
(46) Vericat, C.; Benitez, G. A.; Grumelli, D. E.; Vela, M. E.; Salvarezza, R. C. *J. Phys.: Condens. Matter* **2008**, *20*, 184004–184004.
(47) Cortés, E.; Rubert, A. A.; Benitez, G.; Carro, P.; Vela, M. E.; Salvarezza, R. C. *Langmuir* **2009**, *25*, 5661−5666.
(48) Weitzman, P. D. *Anal. Biochem.* **1976**, *76*, 170–6.
(49) Aqua, T.; Cohen, H.; Vilan, A.; Naaman, R. *J. Phys. Chem. C* **2007**, *111*, 16313–16318.

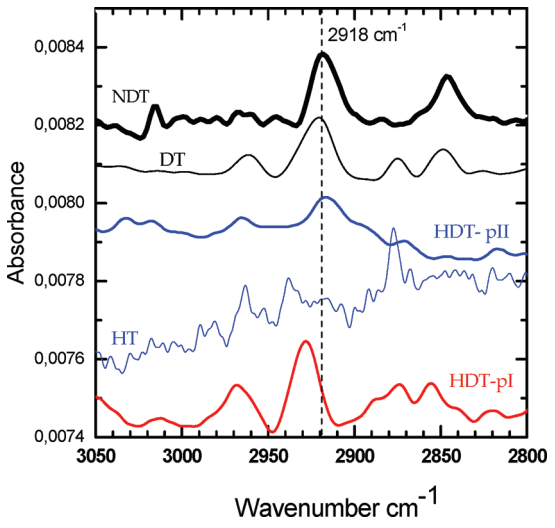

Figure 5. RAIRS spectra for HDT and NDT SAMs prepared by procedure II (in a degassed *n*-hexane solution and in the dark) and for HDT prepared by procedure I. Also shown are spectra for HT and DT SAMs prepared by procedure I.

standing-up phase. The XPS data also show that the NDT SAM prepared by procedure II exhibits a higher fraction of standing-up molecules than that found for HDT SAM prepared under the same experimental conditions.

Finally, for BDT SAMs (Figure 4c,d) only the S 2p 162 eV signal is significant irrespective of the self-assembly procedure. This result clearly indicates that BDT remains mainly chemisorbed in the lying-down configuration with two thiolate-Au bonds per molecule. This behavior differs from that reported for butanethiol on Au (111) for which the dense standing phase is easily obtained.[44] Note that although we observe some E_p shift in the electrochemical data for these samples it is evident that it is not related to disulfide formation, as the contribution of the 163 eV component is negligible.

We can conclude from the electrochemical and XPS data that SAMs prepared by procedure II are of a better quality, as we cannot detect excess in the 163.5 eV component related to disulfide formation, and furthermore the important role of chain length to determine the configuration of the dithiol molecules on the Au (111) surface.

In the following, we investigate the order in the SAMs by RAIRS and the presence of sulfur at the outmost part of the SAMs by TOF-DRS.

3.3. RAIRS Measurements. RAIRS spectra on NDT SAMs grown by procedure II (degassed *n*-hexane and with all processing done in the dark) have been reported previously.[35] Here, we performed similar measurements for HDT and compared with the result of growth by procedure I. The RAIRS spectra for HDT, NDT,[35] and also HT and decanethiol (DT) SAMs are shown in Figure 5. The DT and HT spectra are in agreement with existing literature,[14] with only a weak signal observable for the $\upsilon_{as}(CH_2)$ peak for HT.

The dithiol spectra display a peak corresponding to symmetric $\upsilon_{as}(CH_2)$ at 2918 cm^{-1}. We also observe a peak at 2850 cm^{-1} for the symmetric stretch $\upsilon_s(CH_2)$. As discussed in our previous work,[35] these values correspond to a well-organized SAM. Indeed, in disordered SAMs these values tend to 2926 cm^{-1} and 2855 cm^{-1}, respectively, as in the gas phase.[35]

In RAIRS, we do not observe the SH peak located at 2565 cm^{-1}. As noted previously, this is probably due to the fact that this signal remains weak by comparison to the CH vibration signals, as seen in the gas phase. SH vibrations were observed for the NDT SAM by SFG as reported previously.

The results for the samples prepared by procedure II are reproducible though the quality of assembly judged by RAIRS peak position could vary, with the peak found between 2918 and 2921 cm^{-1} (a variability that can also be observed for alkanethiols). In some cases, we observe rather broad spectra indicating disorder at the SAM, which might be due to some variations in preparation conditions regarding, e.g., degassing. As shown by us previously, without degassing and in presence of light well-ordered SAMs are not obtained.[35]

On the other hand, for HDT SAMs prepared by procedure I (with and without degassing the solution), we could not obtain spectra consistent with well-ordered hydrocarbon chains as shown in Figure 5. In fact, in this case we observe the $\upsilon_{as}(CH_2)$ at 2926 cm^{-1}. Similar results were obtained for NDT SAM prepared by this procedure. The disorganizing effect of ethanol on the order of NT SAMs has also been observed by in situ X-ray diffraction experiments.[50] One can also note that the intensity of the $\upsilon_{as}(CH_2)$ at 2926 cm^{-1} for the HDT SAM is larger than that observed for the HDT SAM prepared by procedure II. This result suggests an excess of molecules, a result consistent with the electrochemical data.

The presence HDT molecules bonded by disulfide S−S bonds at the SAM surface and also extra HDT molecules strongly bonded to the SH terminal group of the layer by S−S bonds (SH-R-S-S-R-S-Au) contribute to the disorder observed by RAIRS.

3.4. TOF-DRS Analysis. TOF-DRS measurements were performed in order to ascertain the presence of sulfur atoms on top of the SAMs. In previous studies,[40] on alkanethiol SAMs we have not detected S atoms both for the lying-down phase and the standing-up phase. In the lying-down phase, chemisorbed S atoms are shadowed by both hydrocarbon chains, and in the standing-up phase, the S atoms lie below the hydrocarbon chain and are not accessible to the Ar ion beam.

The dithiol SAMs prepared from *n*-hexane and ethanol solutions were transferred rapidly into the UHV setup, and time-of-flight measurements of recoiled and scattered particles were performed. Figure 6a shows TOF-DRS spectra for HDT and NDT SAMs acquired at an incidence angle of 5° measured from the surface. This low incidence angle increases the sensitivity of the technique to the outermost top layer of atoms, which is desirable to identify if there are dithiol molecules with the SH group on the top atomic layer, as expected in the case of the standing-up phase. For comparison purposes, a TOF-DRS spectrum of a decanethiol SAM grown in vacuum is also included in Figure 6a.

The spectra of Figure 6a present two intense peaks at low times of flight. These correspond to H and C recoils. At higher times of flight, a very small Ar multiple scattering (MS) peak, corresponding to collisions of the projectile with the adsorbed molecules, can be discerned in the case of the decanethiol (DT) spectrum.[40] For the dithiol SAMs, it is possible to distinguish an additional small broad hump and, in the case of NDT SAM, two more clearly pronounced structures identified in the figure. These structures correspond to Ar scattering on S atoms and to recoiled S atoms, and is clear proof that there are S atoms located at the top of the dithiol monolayer. These results are in agreement with the RAIRS, XPS, and electrochemistry data presented above, and also suggest the formation of standing-up dithiol layers. Note that for the thiol SAM spectrum no hump is observed, since the S atoms are lying below the hydrocarbon chain and are not accessible to the Ar ion beam.

(50) Capitán, M. J.; Álvarez, J.; Calvente, J. J.; Andreu, R. *Angew. Chem., Int. Ed.* **2006**, *45*, 6166–6169.

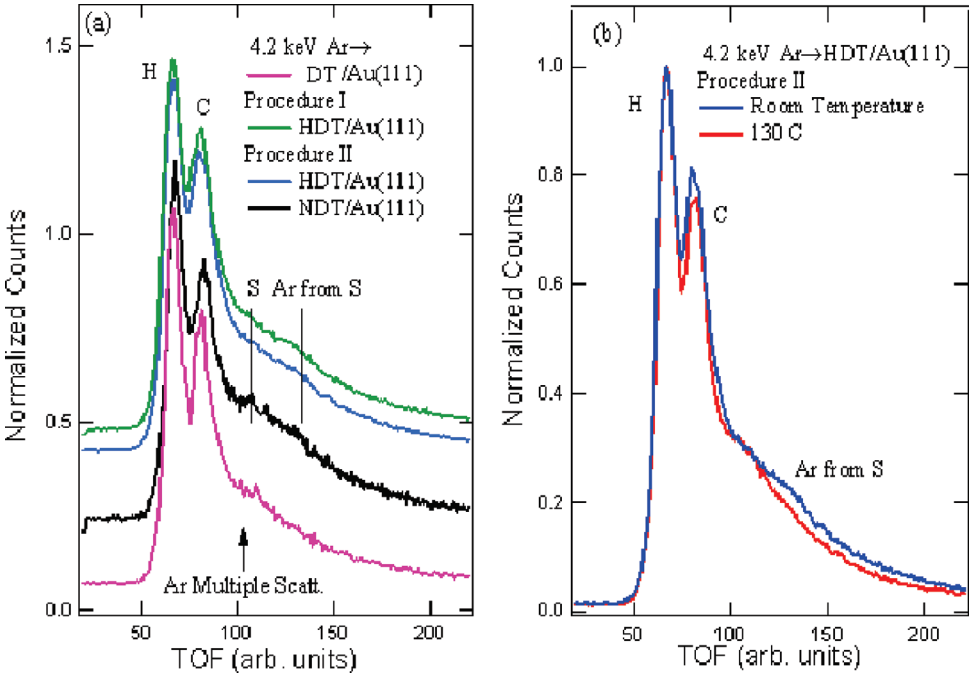

Figure 6. (a) TOF-DRS spectra for Ar scattering on decanethiol (DT), nonanedithiol (NDT), and hexanedithiol (HDT) SAMs taken at room temperature prepared by procedures I and II as indicated. (b) TOF-DRS spectra for Ar scattering on a hexanedithiol (HDT) SAM at room temperature and after increasing the sample temperature to 130 °C.

It should be pointed out that the S features are weak and rather broad, and their intensity varied for different SAMs samples. In comparison, we have found much better defined peaks when the dithiol molecule adsorption was conducted in vacuum conditions (this study will be discussed in greater detail in a forthcoming paper).[51] The weakness of the structures may be related to the partial degradation of the layers when transported from the solution into the vacuum setup. In some cases, no structures could be observed. In our previous paper,[35] we had pointed out that SH vibrational signals could disappear in ambient conditions, because of photooxydation. This could lead to shadowing of sulfur atoms by oxygen.

We also studied alteration in spectra as a function of temperature. For alkanethiol SAMs, it has been noted that a change in the layer structure occurs at about 100 °C. This has been attributed to an initial desorption and disordering of the layer, which may lead to formation of a lying-down phase.[36] In order to investigate the temperature effect, we have heated the dithiol SAM inside the UHV chamber and have observed that the structure associated with S atoms disappeared between 100 and 120 °C. In Figure 6b, we compare the spectrum for the HDT SAM measured at room temperaure (blue line) to the corresponding one measured at 130 °C (red line), where the S hump is not observed. Since with TOF-DRS we cannot detect S from molecules that are in the lying-down phase,[40] this change in the dithiol spectra with temperature could be associated to a partial desorption of alkanedithiol molecules and formation of a lying-down phase similar to that for alkanethiol SAMs.

4. Discussion

Our results obtained by a number of complementary techniques indicate that chemisorbed dithiols prepared by procedure II move from lying-down configuration (BDT) to standing-up configuration (HDT and NDT) as the hydrocarbon chain length is increased. For HDT, we found mixed domains of both phases. These results contrast previous ones for HDT including gas-phase and liquid-phase deposition where it is proposed that the striped phases may act as effective kinetic traps preventing the transition to other denser phases,[36] and also other results suggesting the formation of ordered multilayers.[30] On the other hand, for HDT and NDT prepared by procedure I we also found predominant contributions of the standing-up phases. However, in this case the situation is more complex, as disulfide bridges seem to be formed between the terminal SH groups of the dithiol molecules, and for HDT, we observe the presence of extra dithiol molecules on the layer. In the following, we discuss briefly our results for both methods of preparation we investigated.

4.1. Dithiol SAMs from Procedure II. For NDT and HDT SAMs prepared by procedure II (degassed *n*-hexane solution/dark), the experimental data indicate that the standing-up phase dominates, explaining the TOF-DRS measurements that detect S atoms at the outer part of the SAM. These results for NDT confirm our earlier report based on SFHG, RAIRS, and spectroscopic ellipsometry.[35] The latter indicated formation of a layer whose thickness was compatible with a monolayer. RAIRS results for this procedure indicate formation of well-ordered phases with CH_2 vibrational frequencies lying in the 2918−2921 cm^{-1} range. No evidence of oxidized S species was observed by XPS for SAMs prepared by this procedure, in the absence of oxygen and light. Electrochemical and XPS data suggest the presence of small amounts of lying-down molecule domains, which are smaller for the longer NDT molecules. On the other hand, only the lying-down phase is present in BDT SAMs. These results reveal the crucial role of van der Waals interaction not only in assisting the lying-down to standing-up transition (see below), but also to organize the hydrocarbon chains into well-defined crystalline structures.

The fact that a standing-up phase of dithiols can in fact be produced both from solution and, in particular, in adsorption in vacuum from the vapor phase mentioned above,[51] where other types of molecules present in solutions are absent, might appear

(51) Rodríguez, L. M.; Gayone, J. E.; Sánchez, E. A.; Grizzi, O.; Hamoudi, H.; Esaulov, V. A. to be published.

surprising, since we start with the lying-down phase with both S atoms chemisorbed as thiolates. A possible explanation for the existence of the transition to the standing-up phase could be a hydrogen exchange reaction between an incident free (gas phase, or in solution) dithiol molecule with a chemisorbed lying-down dithiolate on Au. This would result in the liberation of one of the ends of the chemisorbed molecule and chemisorption of the free dithiol leading thus to two standing-up chemisorbed dithiols, i.e.

$$\text{Au-SRS-Au} + \text{HSRSH} \rightarrow 2\text{Au-SRSH} \quad (1)$$

Thereafter, the stability of the standing-up phase would rely on the strength of van der Waals forces. This reaction is now being investigated theoretically.

4.2. Dithiol SAMs from Procedure I. In the case of BDT, we observe the same behavior irrespective of the self-assembly procedure. It means that there is no significant solvent effect and oxygen content in the formation of the lying-down phases, where the molecules are strongly bonded by two thiolates to the substrate. On the other hand, results from HDT and NDT, where the molecules adopt the standing-up configuration, demonstrate that the self-assembly procedure becomes crucial to controlling the structure and chemistry of the SAM, as it affects directly the stability of the free SH groups.

Results for HDT and NDT indicate the existence of disulfide bridges between SAM molecules and some extra molecules bonded to the SAM. It is not surprising that disulfide bridges can be formed in ethanol due to the polar nature of the solvent and the presence of oxygen and traces of water. In this solvent, we observe faster self-assembly kinetics than found in *n*-hexane leading to a charge density consistent with the formation of a monolayer of dithiols in standing-up configuration in few minutes (Figure 2a). After the formation of the standing-up phase, a chemical transformation of the SH end group of some molecules into other chemical species takes place. This leads to formation of dithiol bridges and allows attachment of some extra dithiol molecules, although measurements as a function of immersion time described here did not yield results that would be compatible with formation of progressively thicker multilayers as reported elsewhere by some authors.[30] The extra charge in the reductive desorption measurements, the marked shift in the electrodesorption potential, and the presence of an excess of strongly bonded molecules with S 2p signal at 163.5 eV support disulfide formation at the SAM as already reported.[31,42] It should be noted that similar S 2p XPS spectra with large 163 eV contribution have been reported for octanedithiol SAMs on Au (111) prepared from ethanolic solutions, although the possible presence of disulfide was not discussed.[52]

Now, we discuss the formation of disulfide bridges at the free SH groups of the molecules in the standing-up phase when they are prepared by procedure I. It has been reported that the formation of disulfide bonds between adjacent adsorbed dithiolate molecules at a compact monolayer requires a rotation of 180° of one of the alkyl chains with respect to the other, a process that becomes more difficult as the number of C atoms in the hydrocarbon chain increases.[31] Therefore, one could envisage catalyzed reactions leading to dithiol bridges directly between the adsorbed molecules in disordered regions or at domain boundaries through the reaction

$$\text{Au-SRSH} + \text{Au-SRSH} \rightarrow \text{Au-SRS-SRS-Au} + \text{H}_2 \quad (2a)$$

Therefore, the amount of disulfide bridges should depend on the SAM quality and on the length of the hydrocarbon chains, although obviously both SAM quality and chain length are closely related.[42]

Disulfide bridges could also be formed by reaction of the terminal SH of the chemisorbed molecules with other dithiol molecules present in the solution as suggested in ref 30, activated by molecules in the solvent (O_2, H_2O) and light

$$\text{Au-SRSH} + \text{HSRSH} \rightarrow \text{Au-SRS-SRSH} + \text{H}_2 \quad (2b)$$

In fact, it is well-known that disulfides species are produced by the reaction of aliphatic and aromatic thiol with oxygen in the presence of metal catalysts.[53] The free SH groups of the added disulfide molecules can undergo a new reaction with other dithiol molecules in solution or form looped structures with adjacent chemisorbed molecules of the SAM leading to a complex and disorganized layer.

Therefore, in electrochemistry the reductive desorption in alkaline media not only involves

$$\text{Au-SRS}^- + \text{e} \rightarrow {}^-\text{SRS}^- + \text{Au} \quad (3)$$

but also the contribution of the reactions[54]

$$\text{Au-SRS-SRS-Au} + 4e \rightarrow 2\text{Au} + 2^-\text{SRS}^- \quad (4a)$$

$$\text{Au-SRS-SRS}^- + 3e \rightarrow \text{Au} + 2^-\text{SRS}^- \quad (4b)$$

although another possible pathway is possible

$$\text{Au-SRS-SRS}^{\cdot} + \text{e} \rightarrow \text{Au} + {}^-\text{SRS-SRS}^- \quad (5)$$

The electrochemical cleavage of S−S bonds by reactions 3 and 4 could explain the increase (from ~80 to ~130 μC cm^2) in the electrochemical charge related to reductive desorption and the marked shifting of the reductive desorption peak in the negative direction. In fact, it has been shown that disulfide species are reduced on mercury electrodes at ~0.25 V more negative than the corresponding thiol. Also, reactions 3 and 4 can explain the significant readsorption observed after reductive desorption of this surface structure due to the greater insolubility of longer disulfide species. Note that a bilayer of lying-down molecules can be discarded, because in this case, no S should be detected in the TOF-DRS spectra.[39]

Taking into account this scenario, we discuss our results for NDT in ethanol. We observed that the total amount of molecules is slightly smaller ($\theta_{DS} \approx 0.29$) than that corresponding to a complete standing-up phase ($\theta_{DS} \approx 0.33$). The fact that the amount of charge q is greater than that expected for $\theta_{DS} \approx 0.29$, the E_p shift in the negative direction, and the significant readsorption also point out that certain amount of disulfide is also present in the SAMs. The presence of a certain amount of disulfides bonded to the outer plane of the SAM could explain RAIRS data that show no ordering of the hydrocarbon chains.

5. Conclusions

The results obtained from our multitechnique study about dithiol SAMs on Au (111) indicate that the amount of the lying-down phase decreases sharply from BDT (most lying down) to

(52) Fujita, D.; Ohnishi, K.; Ohgi, T. *Sci. Technol. Adv. Mater.* **2002**, *3*, 283–287.

(53) Arisawa, M.; Sugata, C.; Yamaguchi, M. *Tetrahedron Lett.* **2005**, *46*, 6097–6099.

(54) Kizek, R.; Vacek, J.; Trnkova, L.; Jelen, F. *Bioelectrochemistry* **2004**, *63*, 19–24.

NDT (most standing up) irrespective of the self-assembly procedure. A good ordering of the hydrocarbon chains in the standing-up configuration is observed for NDT when the system is prepared in degassed *n*-hexane with all operations carried out in the dark. These results agree with a previous study by some of us for NDT using RAIRS, SFG, and spectroscopic ellipsometry.[35]

A chemical reaction involving hydrogen exchange between an incident free dithiol molecule with a chemisorbed lying-down dithiolate on Au that could explain the transition process from the lying-down phase to standing-up phase is proposed.

In contrast to previous results, we find that HDT SAMs also exhibit a significant contribution of molecules in the standing-up phase. Our data for self-assembly by procedure I also point to the formation of disulfide bridges at the free SH terminal groups at both HDT and NDT SAMs. However, we found no evidence of ordered multilayer formation in our experiments. No disulfides were observed for BDT, which only form the lying-down phase, prepared by procedure I. Our results demonstrate the key role of chain length and procedure (solvent nature and oxygen presence) in controlling the surface structure and chemistry of dithiols SAMs on Au (111), and explain contradictory results found in the literature for these systems.

Acknowledgment. We acknowledge financial support from ANPCyT (Argentina, PICT06-621, PAE 22711, PICT06-715), SeCyT (Argentina) − ECOS (France) Program (no A07E01) and U.N. Cuyo. M. E. Vela is a member of the research career of CIC BsAs. R.C.S is a Guggenheim Foundation Fellow.

Self-assembled dithiothreitol on Au surfaces for biological applications: phospholipid bilayer formation

Tânia B. Creczynski-Pasa,[a] M. Antonieta Daza Millone,[b] Maximiliano L. Munford,[c] Vânia R. de Lima,[a] Tiago O. Vieira,[a] Guillermo A. Benitez,[b] André A. Pasa,*[a] Roberto C. Salvarezza[b] and María E. Vela*[b]

Received 17th July 2008, Accepted 5th November 2008
First published as an Advance Article on the web 24th December 2008
DOI: 10.1039/b811964c

Self-assembly of dithiothreitol (DTT) on Au(111) from solution deposition has been studied by X-ray photoelectron spectroscopy and electrochemical data. DTT molecules self-assemble on Au(111) in a lying-down configuration irrespective of the concentration and temperature. XPS and electrochemical data indicate a DTT surface coverage of $\theta \approx 0.16$ with two S-head–Au covalent bonds per DTT molecule. The DTT monolayer turns the Au surface hydrophilic enough to allow the formation of fluid dimyristoylphosphatidylcholine (DMPC) bilayer domains by vesicle fusion as revealed by *in situ* atomic force imaging. Methylene blue (MB) and flavin adenine dinucleotide (FAD) have been used as probes to study molecule transport across the bilayer.

1. Introduction

Lipid membranes of living cells are the most important barriers to control the majority of cellular processes. They play a fundamental role in cell-to-cell communication involving the exchange of ions and biomolecules, including calcium, neurotransmitters, proteins, reactive species, and drugs among others.

Phospholipid bilayers can be taken as a model system of cell membranes because they preserve 2-D fluidity and can be modified with membrane proteins, ion channels, receptors and transporters, and can be used for various biotechnological applications.[1–3] Liposomes, in which phospholipid composition, structure and dynamics can be fully controlled, are generally accepted as a suitable model for *in vitro* studies of cell membrane structures and properties.[4–6] Liposomes are vesicles formed by a lipidic bilayer, structurally similar to the lipidic matrix of a cell membrane. However, to perform studies with atomic force microscopy (AFM), a technique that allows the determination of morphological and mechanical properties of structures, the immobilization of the lipidic bilayer on a solid surface[7–10] is required. There exist several methods to spread phospholipids on a solid substrate in order to achieve a supported bilayer.[11] Among the most widely used methods are sequential transfer of two monolayers from the air–water interface *via* Langmuir–Blodgett (LB) and Langmuir–Schaefer (LS) techniques,[12,13] single bilayer spreading[14] and vesicle fusion.[15]

Lipidic membranes supported on inorganic material surfaces, *e.g.* gold and mica, yield important results related to phase transition, stability and morphology of the layers and are promising structures for the development of biosensors.[16–18] On these surfaces, however, the physical–chemical properties of the lipidic layers are significantly different from membranes in fluid environments.[19] A promising approach is to use self-assembled monolayers (SAMs) of thiol molecules on gold, since they can act as a bridge or a spacer between the inorganic surface and the assembled macromolecules. Modification of solid surfaces with a spacer to link phospholipids bilayers provides a selective anchoring layer to accommodate hydrophilic domains of proteins and enables the charge transport from one side of the membrane to the other side.[4–6,20]

Concerning the inorganic surface there is a particular interest in metallic substrates because they can be used as electrodes in electrochemical-based biosensors. Gold substrates are particularly attractive because they are biocompatible and inert materials that can be modified by simple solution chemistry without significant contamination.

Several approaches have been developed to support phospholipid bilayers on gold. Hybrid bilayers of phospholipids on alkanethiol[21] or thiophospholipid[22] SAMs on gold lead to well ordered and blocking artificial membranes but they lack a proper fluidity to resemble a biomimetic system. Adding a long thiolated linker to the phospholipid tethered bilayers[5,6] or performing vesicle fusion over long ($C_n > 11$) hydroxyl-terminated thiols[20,23] (as a hydrophilic surface is required for this strategy) improve fluid properties. However an increase in the length of the linker chain should hinder electron transfer.[24] Therefore the use of a very short spacer that turns the gold surface hydrophilic enough for vesicle fusion and allows an easy electron transfer should be a suitable choice to build an electrochemical biosensor. Unfortunately, short hydroxyalkanethiol SAMs, *e.g.* 2-mercaptoethanol, have a lower stability against reductive desorption[25] which greatly decrease the range of electrochemical sensing ability.

[a] *Departamento de Ciências Farmacêuticas and Departamento de Física, UFSC, C. P. 476, Florianópolis, 88.040-900, Brazil. E-mail: pasa@fisica.ufsc.br; Fax: +55 48 3234 0599*
[b] *INIFTA, CONICET-UNLP, La Plata, CC 16 Suc. 4, Argentina. E-mail: mevela@inifta.unlp.edu.ar; Fax: +54 221 425 4642*
[c] *Departamento de Física, UFV, Viçosa, Brazil*

According to the previously mentioned requirements, dithiothreitol (DTT) appears to be a good candidate for these purposes. In fact, it is a short α,ω-alkanedithiol with two hydroxyl groups that, if the molecule adopts a lying-down configuration, should be exposed to the environment (Fig. 1). DTT SAMs have been used to bind Ag^+ cations,[26] to immobilize gold nanoparticles,[27] to study heterogeneous binding of divalent metals,[28] and also to provide an hydroxylated substrate for sol–gel synthesis.[29] It has been reported that DTT self-assembly on Au(111) changes the contact angles of a water droplet on gold from 50° to 38°.[30,31] Also, a related molecule, cyclo-DTT enabled the formation of an hierarchical self-assembly of proteins to a gold surface *via* the disulfide moiety and opening the S–S bond.[32]

In this work, we have used DTT as a sulfur bridge to separate the lipidic membranes from the gold surface. DTT self-assembled monolayers on Au(111) were characterized by its electrodesorption curves. Results from scanning tunneling microscopy (STM) show that DTT molecules induce the formation of the typical monoatomic deep pits.[33] From X-ray photoelectron spectroscopy (XPS) data we can conclude that DTT molecules self-assemble in a lying down configuration. The OH-rich surface facilitates the formation of fluid dimyristoylphosphatidylcholine (DMPC) bilayer domains obtained by vesicle fusion as observed by *in situ* atomic force measurements (AFM). Electrochemical results using two molecular probes, methylene blue (MB) and flavin adenine dinucleotide (FAD), confirm that a continuous and fluid bilayer is formed on the DTT–Au surface.

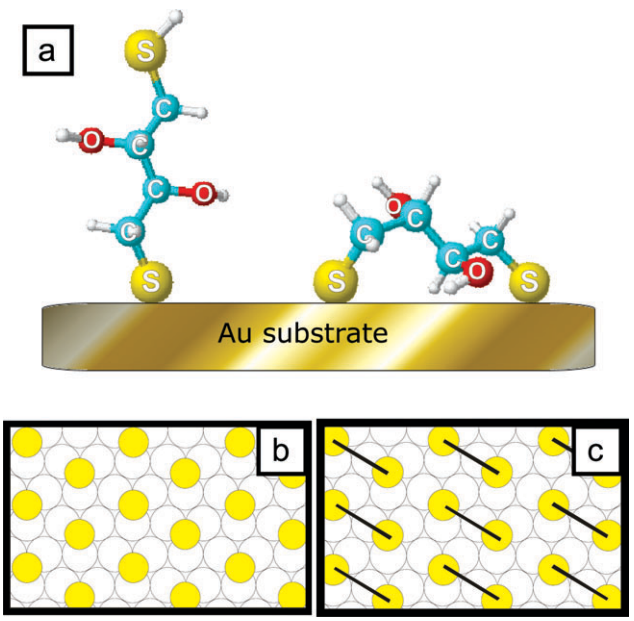

Fig. 1 (a) Representation of the DTT molecule according to a calculation using a PM3 semiempirical method. Each atom is labeled except hydrogens (white spheres). Standing up (left) and lying down (right) conformations. (b) $\sqrt{3} \times \sqrt{3}$ R30° structure for S heads (top circles) in the standing up configuration on the Au(111) substrate (white circles). (c) Lying down configuration of the bidentate molecules with S heads in a $\sqrt{3} \times \sqrt{3}$ R30° lattice.

2. Experimental

2.1 Substrates

Two different types of Au substrates were used. The first one was 250 nm thick gold films prepared by physical vapor deposition on a 4 nm chromium layer on glass (Gold Arrandee™). A three minute flame annealing was performed to generate a substrate consisting of atomically flat Au(111) terraces (Fig. 2a), separated by monoatomic steps. In these flat terraces atomic resolution of the Au(111) surface can be reached (Fig. 2b and inset). However, the root mean square roughness (rms) measured over 10 μm × 10 μm images is ≈12 nm due to the presence of deep grain boundaries between the atomically smooth large crystals. These substrates were used to study the self-assembly of DTT and to compare these results with those obtained for butanethiol monolayers. After DTT adsorption the typical monoatomic and diatomic deep pits formed during thiol self-assembly are observed (Fig. 2c, arrows).

The second type of substrates were thin films of vapor-deposited Au on silicon. The film consists of small grains of 20 nm in average size (Fig. 2d). Typical root mean square roughness values measured on 10 μm × 10 μm images are ≈3 nm. This substrate was used to prepare the phospholipid bilayers due to its low surface roughness and the absence of deep grain boundaries.

2.2 Chemicals

DL-Dithiothreitol (DTT), 1-butanethiol, 4-(2-hydroxyethyl)-1-piperazineethanesulfonic acid (HEPES) and flavin adenine

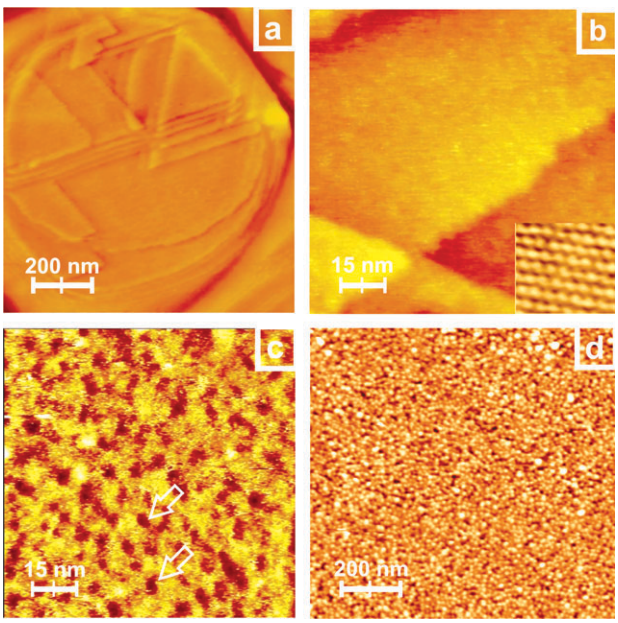

Fig. 2 (a) *Ex situ* 1 μm × 1 μm STM image of Au Arrandee™ substrate after H_2 flame annealing. (b) 75 nm × 75 nm STM image of smooth Au (111) terraces where atomic resolution is observed (inset 1.7 nm × 1.7 nm). (c) *Ex situ* 75 nm × 75 nm STM image of Au Arrandee™ substrate after incubation in 50 μM DTT ethanolic solution during 30 min at 60 °C. Note the formation of the typical pits produced by DTT adsorption (arrows show a couple of them). (d) *Ex situ* 1 μm × 1 μm AFM image of gold evaporated on Si(100). The image shows that the sample consists of grains ~20 nm in size.

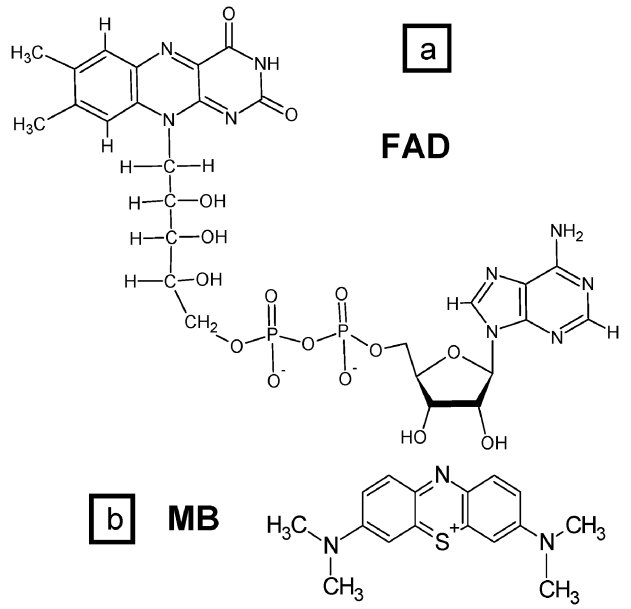

Fig. 3 (a) Flavin adenine dinucleotide and (b) methylene blue, both in their oxidized forms.

dinucleotide (FAD, Fig. 3a) were purchased from Sigma, dimyristoylphosphatidylcholine (DMPC) was purchased from Avanti and methylene blue (MB, Fig. 3b) from Merck. All other supplies used were of the best analytical grade commercially available.

2.3 Self-assembly and characterization of DTT SAMs

DTT SAMs were prepared by immersion of the gold substrates in 5 mM or 50 μM DTT ethanolic solution either at 25 °C or 60 °C for different times (t). Blank experiments using 50 μM butanethiol ethanolic solutions were also performed.

DTT SAMs were then analyzed by XPS, electrochemical measurements and *ex situ* STM. XPS measurements were performed using an Mg-Kα source (XR50, Specs GmbH) and a hemispherical electron energy analyzer (PHOIBOS 100, Specs GmbH). Spectra were acquired with 10 eV pass energy and a Shirley-type background was subtracted to each region. A two point calibration of the energy scale was performed using sputtered cleaned gold (Au 4f 7/2, binding energy = 84.00 eV) and copper (Cu 2p 3/2, binding energy = 933.67 eV) samples. C 1s at 285 eV was used as charging reference.

STM measurements were carried out with a Nanoscope IIIa (Veeco, Santa Barbara, USA). The presence of etched pits characteristic for chemisorption of thiols on gold are clearly visible (Fig. 2c). No molecular resolution was achieved under the experimental conditions used in this work.

Electrochemical measurements were performed in a conventional glass-made cell using the DTT-covered Au substrate as working electrode and a large Pt plate and a saturated calomel electrode as counter and reference electrodes, respectively, using a TEQ-2 potentiostat with data acquisition capability. Solutions were prepared with analytical-grade chemicals and Milli-Q water.

Reductive desorption measurements of DTT and butanethiol self-assembled monolayers were made following the procedure described elsewhere.[34,35] Briefly, a potential sweep was applied to the SAM-covered Au substrate immersed in a three-electrode electrochemical cell containing 0.1 M NaOH at 0.05 V s^{-1} from −0.4 V to −1.4 V.

Each solution was freshly prepared just before each series of measurements and deaerated with purified nitrogen.

2.4 Self-assembly of phospholipidic bilayers on DTT-covered Au substrates

DTT-covered Au prepared from 50 μM ethanolic solution at 60 °C for t = 30 min were used as substrates for supported bilayer formation by vesicle fusion.[30]

DMPC vesicles were obtained by evaporating, under a stream of nitrogen, the solvent of a phospholipidic solution (10 mg mL^{-1}) prepared in chloroform. The samples were dried under vacuum to eliminate solvent traces. Subsequently, multilamellar vesicles were obtained by the addition of a buffer containing 10 mM HEPES + 0.9% NaCl and vortexing. The multilamellar suspension was then extruded through a polycarbonate filter with 400 nm pore from Nuclepore to form unilamellar vesicles.[36,37]

DTT-covered Au substrates were immersed in 10 mg mL^{-1} DMPC unilamellar vesicle suspension for 90 min at ~30 °C (above DMPC phase transition temperature T_m = 23.9 °C) to allow vesicle fusion. The samples were then fast rinsed with 10 mM HEPES + 0.9% NaCl solution to remove the unbounded lipids, and immediately transferred to the AFM liquid cell. All AFM measurements were performed at pH 7.4 with a Molecular Imaging PicoScan microscope inside the fluid cell with temperature control, *i.e. in situ*, containing 10 mM HEPES + 0.9% NaCl, under contact mode with silicon nitride probes (triangular cantilevers with nominal spring constant of 0.12 N m^{-1}, Veeco Probes). The images were analyzed using the program VS × M 2.1 (Nanotec Electronica).

2.5 Electrochemical measurements with redox biomolecules

The experiments with the redox couples were performed in phosphate buffer 0.1 M pH = 7.0. The DTT–Au electrodes with or without the phosphilipidic bilayer were dipped in 0.1 mM methylene blue (MB) or 0.1 mM flavin adenine dinucleotide (FAD) aqueous solutions for 30 min at T = 37 °C. Potentials in the text are referred to the saturated calomel electrode (SCE).

3. Results and discussion

The self-assembly of DTT (DL-dithiothreitol) can be compared with the well-known self-assembly of short alkanethiolates. In principle, the DTT molecule can adopt two different configurations (standing up or lying down) on the Au(111) surface as schematically shown in Fig. 1a. Possible surface structures for those configurations considering the well-known surface structure reported for thiols,[33,38] dithiols[39–41] and DTT on Au(111)[30] are depicted in Fig. 1b and c.

Typical XPS data obtained for DTT-covered Au(111) surfaces prepared by immersion in 50 μM ethanolic solutions for t = 30 min at T = 60 °C are shown in Fig. 4a. After self-assembly, the sample was removed from the solution, carefully

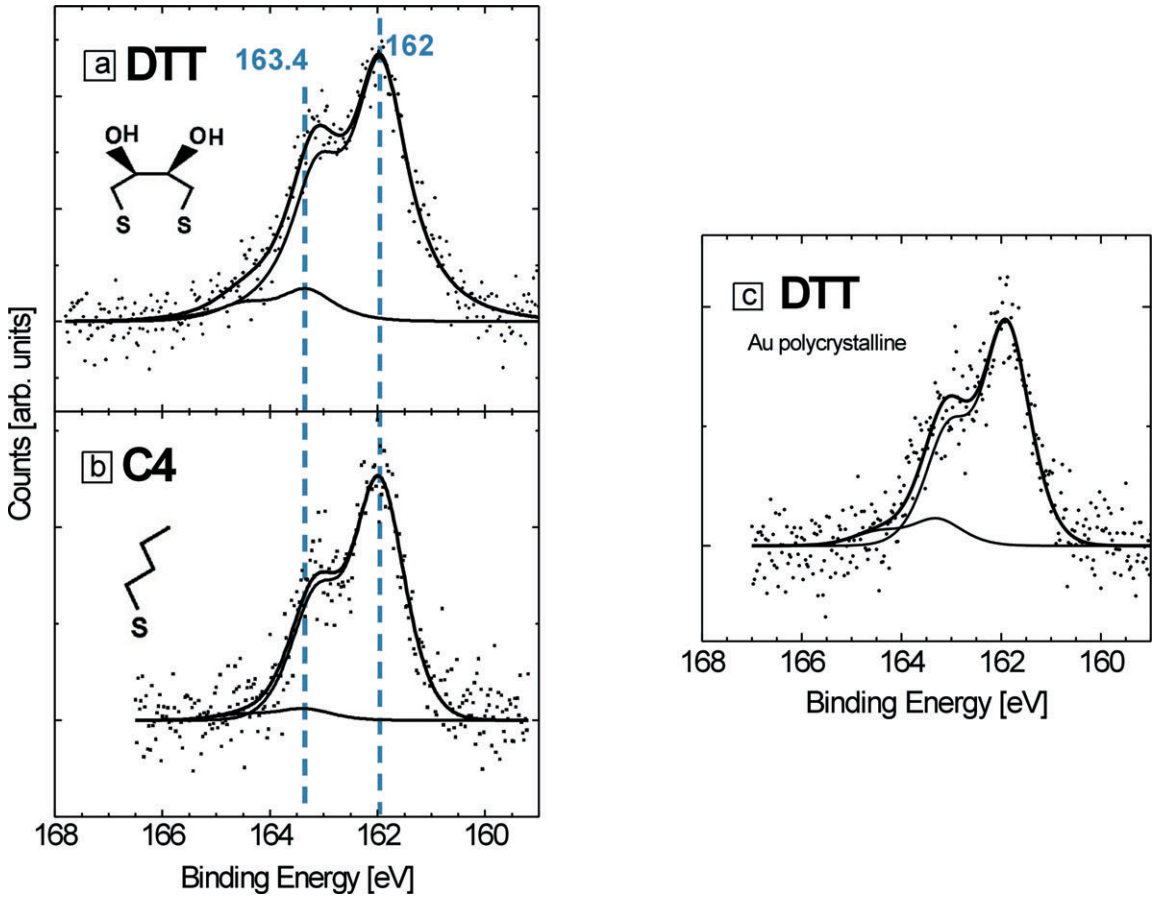

Fig. 4 XPS spectra (S 2p) taken from different thiol adlayers: (a) 30 min DTT 50 μM at 60 °C on Au(111), (b) 24 h butanethiol 50 μM at 25 °C on Au(111), (c) DTT on polycrystalline gold, incubated with the same conditions as for (a). Experimental points are represented by dots and the best fits by a continuous line. Main contributions are marked with dashed lines.

rinsed with ethanol and dried under a nitrogen flux before transferring to the UHV chamber. A broad XPS S 2p signal at 162–163 eV can be observed, a clear indication that thiols are present on the gold surface.[42] The S 2p signal was fitted by two doublets at 162 eV and 163.4 eV. The main component at 162 eV (Fig. 4a) corresponds to the S-head–Au covalent bonds as already reported[43] for different thiols on metal surfaces.[42] The smaller doublet at 163.4 eV corresponds to free SH groups which can be assigned either to physisorbed molecules that remain on the sample after the cleaning procedure or a small amount of molecules in standing up configuration (Fig. 1a).

Therefore, it can be concluded that the DTT molecules are chemisorbed mainly in a lying down configuration with two S-head–Au bonds per molecule (Fig. 1a, right). In fact, for DTT in the standing up configuration (Fig. 1a, left) we expect a significant contribution of the SH signal at 163.4 eV, which in this case is a minor contribution.

The S 2p (162 eV)/Au 4f signal ratio is a measure of the chemisorbed thiol coverage. We have used a self-assembled monolayer (SAM) formed on Au(111) by immersion in 50 μM butanethiol (C4) ethanolic solutions for $t = 24$ h (Fig. 4b) as reference system because, in this case, the SAM reaches its maximum surface coverage value $\theta \approx 0.33$, which corresponds to a $\sqrt{3} \times \sqrt{3}$ R30° surface structure of alkanethiol molecules in standing up configuration. Note that even in this case a small contribution of physisorbed thiol molecules at 163.4 eV is observed. In the C4 SAM (Fig. 4b) the S 2p (162 eV)/Au 4f signal ratio is ≈0.07. The spectrum shown in Fig. 4a for the DTT SAM also shows a S 2p/Au 4f signal ratio ≈0.07, which for a dithiol in the lying down configuration (Fig. 1, right) implies $\theta = 0.16$. Similar results were obtained using a higher concentration (5 mM) either at the same temperature ($T = 60$ °C) or lower ($T = 25$ °C) although for this concentration a greater contribution of the 163.4 eV component was observed. On the other hand, attempts to prepare the DTT SAM from 50 μM ethanolic solution at 25 °C for a self-assembly time of 30 min failed because we found a smaller S/Au ratio, *i.e.* the SAM does not completely cover the Au substrate. Based on the previous results we select 50 μM and 60 °C as the best experimental conditions to form a dense layer of lying down DTT molecules able to turn the Au highly hydrophilic.

In all cases the XPS spectra (Fig. 4) show no traces of oxidized S, such as sulfonates, since no signal was observed at 167–168 eV. Ageing of the sample in ambient condition leads to degradation of the DTT layer characterized by a strong S 2p signal at binding energies >167 eV. It is interesting to note that all DTT samples exhibit a clear O 1s signal contribution arising from the OH groups of the DTT molecules (data not shown).

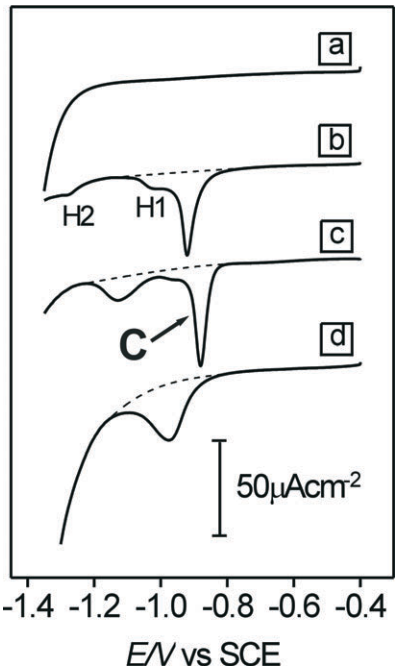

Fig. 5 *j vs. E* profiles for the reductive desorption of DTT and butanethiol SAMs. (a) Bare Au(111), (b) Au(111) incubated 30 min in DTT 50 μM at 60 °C, (c) Au (111) 24 h in butanethiol 50 μM at 25 °C and (d) polycrystalline gold 30 min in DTT 50 μM 60 °C. Measurements were made in NaOH 0.1 M at a sweep rate of 0.05 V s^{-1}.

We have obtained the same XPS results for DTT self-assembled on a vapor-deposited polycrystalline Au substrate (lying down configuration, $\theta = 0.16$) as can be seen in Fig. 4c. The self-assembly of a DTT monolayer on this surface is important for the preparation of continuous lipidic bilayers. As was mentioned in the Experimental section, polycrystalline Au (see Fig. 2d) exhibits a smooth surface consisting of nanometer-sized grains. On the other hand, preferred oriented Au(111) substrates have atomically smooth surface but they have deep grain boundaries that may produce discontinuities in the DMPC bilayer.

We have performed reductive electrodesorption curves to confirm the presence of the DTT covalently attached to the gold substrate. The electrolyte used in this case was NaOH 0.1 M because at neutral pH the current peak related to the thiol electrodesorption overlaps partially with the hydrogen evolution reaction (HER). The cathodic polarization curve shown in Fig. 5a corresponds to a clean (thiol SAM-free) preferentially oriented Au (111) substrate recorded from −0.4 to −1.4 V. Typical double layer response of gold, without any Faradaic current contributions, is observed preceding the large cathodic current related to HER. Fig. 5b shows typical curves recorded for DTT-SAM on the Au(111) prepared from the 50 μM ethanolic solutions for $t = 30$ min at $T = 60$ °C.

These polarization curves are compared with those obtained for butanethiol SAMs prepared by immersing the Au(111) substrate in 50 μM butanethiol ethanolic solution at 25 °C for 24 h (Fig. 5c). We have also included the polarization curve corresponding to a DTT SAM on polycrystalline Au prepared from 50 μM ethanolic solutions for $t = 30$ min at $T = 60$ °C (Fig. 5d).

In all cases, the current/potential profiles recorded for the thiol SAM-covered Au substrates show well defined cathodic current peaks followed by one or two humps preceding HER. As already reported the main cathodic current peak C corresponds to the reductive thiol desorption from the Au surface according to the reaction:[33]

$$1\bar{e} + \text{Au(111)–S–R} \rightarrow \text{R–S}^- + \text{Au(111)} \qquad (1)$$

Note that the current peak recorded for DTT electrodesorption from the polycrystalline Au is broader than those recorded in the preferred (111) oriented substrate due to the presence of different crystallographic faces, grain boundaries and large amount of defects.

First, we analyze the information related to the main peak C in Fig. 5. The peak potential (E_p) for DTT desorption from the Au(111) surface (Fig. 5b) is slightly negative in relation to that measured for a butanethiol (C4) SAM on the same substrate (Fig. 5c). Integration of the current involved in the electrodesorption peaks gives the charge density (q) corresponding to the amount of chemisorbed species. We have obtained a charge density of 73 ± 10 μC cm^{-2} which is consistent with S-head–Au bonds coverage ≈0.33 taking into account reaction (1) (one electron per chemisorbed sulfur atom) and a $\sqrt{3} \times \sqrt{3}$ R30° surface structure on the Au(111) surface. Note that this q value can be expected either for the DTT molecules chemisorbed in standing up ($\theta = 0.33$) or lying down ($\theta = 0.16$) configurations. Nevertheless, the standing up configuration is incompatible with XPS results (Fig. 4a).

Besides the main peak C, two humps H1 and H2 are observed at more negative potentials for DTT-SAM on Au(111). H1 is located on the negative side of the main desorption peak while H2 appears at −1.2 V. In contrast, only a small peak rather than a hump at −1.1 V is observed for butanethiol electrodesorption. This peak has been assigned to thiol molecules strongly chemisorbed at defects of the Au(111) surface such as steps.[44] Therefore, hump H2 can be assigned to DTT molecules adsorbed on Au defects. However, at present we have no clear interpretation on the origin of hump H1.

We have imaged the DTT SAM-covered Au samples by STM. Unlike butanethiol SAMs that exhibit the well-known $\sqrt{3} \times \sqrt{3}$ R30° and c(4 × 2) surface structures,[45] no molecular resolution could be achieved with DTT SAMs. As reported previously, this could be attributed to a more disordered layer.[30] However, DTT SAM formation can be inferred from the presence of the typical nanometer sized monoatomic and diatomic deep pits (Fig. 2c).

In principle, the lying down phase of DTT molecules (Fig. 1a, right) could provide a hydrophilic environment for anchoring different types of biomolecules. In the next paragraph we show that the DTT-SAMs can be used to form ordered phospholipidic bilayer domains on the polycrystalline Au surfaces. As mentioned above these substrates are particularly suitable for the formation of high quality bilayers due to its low roughness (Fig. 2d).

Fig. 6a–c shows *in situ* AFM images in buffer HEPES pH = 7.4 NaCl 0.9% of a vapor deposited polycrystalline Au covered by a DTT-SAM after immersion in a suspension of DMPC vesicles.

The surface morphology of the lipidic bilayer on DTT-SAM has the same characteristics (rms, grain size, *etc.*) as those exhibited by the clean polycrystalline Au substrate (Fig. 2d in Experimental section). As shown in Fig. 6a, large size areas (more than 10 μm × 10 μm) were *in situ* scanned with the AFM tip remaining stable during the time period of the experiments (≈4 h). In order to determine the presence of the lipidic layer we have used a lithographic step by applying an additional force to the cantilever probe. This procedure removes the material present in the scanned region opening a clear squared window, as displayed in Fig. 6b. This evidences that a soft material deposit covers the DTT–Au surface. In fact, complementary XPS data (not shown) of these samples reveal P, N and C, supporting the presence of a DMPC layer.

A line scan through the opened window region (Fig. 6b) provided a thickness of about 5 nm (Fig. 6d). Note that this value is slightly higher than the expected value for a DMPC bilayer (Fig. 7) due to the hydration of the DTT–DMPC interface.[8] It is interesting to note that on clean Au we were unable to form a lipidic layer since vesicles remained sphere-shaped on the surface. In consequence, a highly hydroxylated surface is needed for vesicle fusion necessary to form a bilayer film.

We have also been able to image the self-healing of this layer by lateral motion of phospholipids indicating that it is not rigid at 22 °C (Fig. 6c). The sequential AFM images allow a rough estimation of the lateral diffusion coefficient (D) of the phospholipids of the window (Fig. 6b and c). Taking a front displacement L for the time interval Δt and using $L^2 = 2D\Delta t$ we obtained $D \cong 10^{-11}$ cm^2 s^{-1}. This value is somewhat lower than that reported for DMPC bilayers supported on glass at this temperature (2×10^{-10} cm^2 s^{-1}).[46] The discrepancy can be explained either by a self-limiting spreading as discussed by Boxer[47] or by an increased interaction of DMPC with the underlying DTT/Au with respect to the glass substrate used by Smith *et al.*[46]

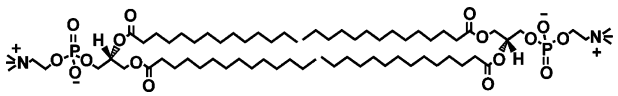

Fig. 7 Scheme showing two DMPC molecules linked by their lipidic tails.

The DMPC lateral motion points toward the maintenance of membrane dynamics, which is a signal that this system could be adequate for fundamental studies in general phenomena of natural membranes, such as the incorporation of biomolecules (enzyme cofactors, proteins, drugs, *etc.*).

Concerning this point, we have tested the behavior of our DMPC bilayer–DTT–Au arrangement when it was exposed to two electrochemically active molecules: methylene blue (MB), a lipophilic molecule able to penetrate biological membranes, and flavin adenine dinucleotide (FAD), an electron carrier, that is known to be unable to diffuse across the membrane.[48,49] The DMPC bilayer–DTT–Au substrates were immersed for 30 min in an aqueous solution containing MB or FAD at 37 °C in order to immobilize these molecules in the fluid bilayer. Afterwards, the substrates were removed from the solution, carefully rinsed with water to eliminate the MB and FAD molecules weakly bonded to the bilayer, and finally immersed in an electrochemical cell containing phosphate buffer at pH = 7.0 to detect the presence of the redox couples corresponding to immobilized molecules. The electrochemical response of the DMPC bilayer–DTT–Au substrates exposed to MB or FAD molecules was also compared to that exhibited for the bilayer-free DTT–Au substrates exposed to the same molecules under the same experimental conditions.

The voltammetric profiles (Fig. 8, dotted lines) show that the DTT–Au substrates have been able to immobilize certain amount of MB and FAD molecules since their redox couples are clearly observed.

On the other hand, for the DMPC bilayer–DTT–Au system only the redox couple of MB is electrochemically detected (Fig. 8, solid line) indicating that these molecules have been incorporated into the phospholipidic bilayer. The more irreversible electrochemical response of trapped MB into the bilayer demonstrates that they are placed at a larger distance from the DTT–Au substrate than in the absence of the bilayer. When FAD molecules are used as electrochemical probes, no electrochemical response is observed, *i.e.* they are not incorporated in the DMPC bilayer.

The electrochemical behavior of these molecular probes demonstrates the continuity and fluidity of our supported bilayers.

Bilayer continuity can be tested using the FAD probe. It is well established that FAD can not diffuse across membranes due to the presence of the pyrophosphate group[48] (Fig. 3a).

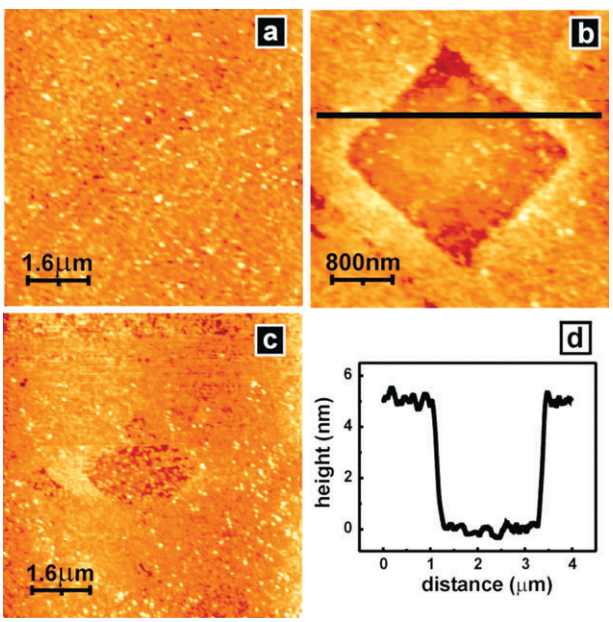

Fig. 6 AFM images of DMPC bilayer formed on a lying down DTT SAM formed on polycrystalline gold. (a) Large covered area with a lipid layer. (b) Square window defined by the removal of the lipid layer using the AFM tip. (c) DMPC layer recovering the surface of the square window, taken 120 s after image (b). (d) Cross section profile corresponding to the black line of image (b).

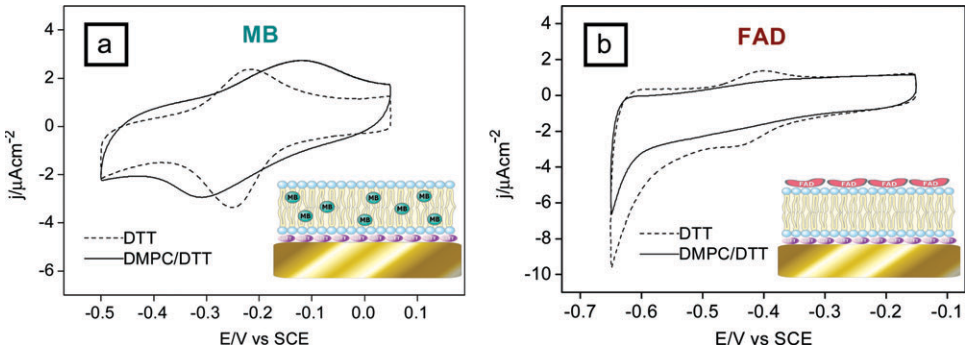

Fig. 8 Selective permeation of biomolecules. Cyclic voltammograms performed in phosphate buffer 0.1 M pH 7.0 at scan rate: 0.05 V s^{-1}. Full lines correspond to voltammograms for DMPC bilayer–DTT–Au (111) substrates incubated 30 min either in MB 0.1 mM (a) or FAD 0.1 mM (b) aqueous solutions to immobilize these molecules. Dotted lines correspond to the voltammograms recorded for DTT–Au(111) electrodes subjected to the same procedure.

FAD could only reach the DTT–Au interface and be electrochemically detected if significant defects like pores or discontinuities were present in the bilayer.

In addition to *in situ* AFM measurements, the MB probe permits fluidity testing. Diffusion of liposoluble molecules through rigid crystalline bilayers would be largely impeded.

4. Conclusions

* DTT molecules self-assemble on Au(111) mainly in a lying down configuration irrespective of the concentration and temperature. XPS and electrochemical data indicate a DTT surface coverage $\theta = 0.16$ with two S-head–Au covalent bonds per DTT molecule.

* The charge density involved in the electrodesorption curves for the DTT SAMs is the same that found for alkanethiols SAMs because the number of S-head–Au bonds remains constant.

* The peak potential for electrodesorption indicates that the stability of the DTT SAM is similar to that observed for butanethiolate SAM.

* DTT-SAMs on Au (111) are not highly ordered as no molecular resolution by STM was found during our STM imaging.

* DMPC bilayer membranes can be formed on DTT–Au because the surface is highly hydroxylated. The membranes exhibit self-healing behavior.

* The DMPC–DTT–Au system was used to test electrochemically the transport behavior of methylene blue and FAD across the bilayer, verifying that it is both fluid and continuous.

Acknowledgements

The authors wish to thank FAPESC, CAPES, CNPq/MCT, CONICET, ANPCyT (PICT 06-621, PAE 22771), for research grants and fellowships. V. R. de Lima is currently a PhD student of the Programa de Pós-Gradução em Química, UFSC. M. E. Vela is member of the research career of CIC BsAs.

References

1 Y. H. Chan and S. G. Boxer, *Curr. Opin. Chem. Biol.*, 2007, **11**, 581–587.
2 E. T. Castellana and P. S. Cremer, *Surf. Sci. Rep.*, 2006, **61**, 429–444.
3 R. P. Richter, R. Berat and A. R. Brisson, *Langmuir*, 2006, **22**, 3497–3505.
4 H. Lang, C. Duschl and H. Vogel, *Langmuir*, 1994, **10**, 197–210.
5 R. Naumann, A. Jonczyk, C. Hampel, H. Ringsdorf, W. Knoll, N. Bunjes and P. Gräber, *Bioelectrochemistry and Bioenergetics*, 1997, **42**, 241–247.
6 N. Bunjes, E. K. Schmidt, A. Jonczyk, F. Rippmann, D. Beyer, H. Ringsdorf, P. Gräber, W. Knoll and R. Naumann, *Langmuir*, 1997, **13**, 6188–6193.
7 J. Schneider, Y. F. Dufrene, W. R. Barger, Jr and G. U. Lee, *Biophys. J.*, 2000, **79**, 1107–1118.
8 F. Tokumasu, A. J. Jin and J. A. Dvorak, *J. Electron. Microsc. (Tokyo)*, 2002, **51**, 1–9.
9 T. Spangenberg, N. F. De Mello, T. B. Creczynski-Pasa, A. A. Pasa and H. Niehus, *Physica Status Solidi (A) Applied Research*, 2004, **201**, 857–860.
10 M. L. Munford, V. R. Lima, T. O. Vieira, G. Heinzelmann, T. B. Creczynski-Pasa and A. A. Pasa, *Microscopy and Microanalysis*, 2005, **11**, 90–93.
11 E. Sackmann and M. Tanaka, *Trends Biotechnol.*, 2000, **18**, 58–64.
12 L. K. Tamm and H. M. McConnell, *Biophys. J.*, 1985, **47**, 105–113.
13 A. Ulman, *An Introduction to Ultrathin Organic Films From Langmuir-Blodgett to Self-Assembly*, Academic Press, Inc., San Diego, 1991.
14 J. Raedler, H. Strey and E. Sackmann, *Langmuir*, 1995, **11**, 4539–4548.
15 A. A. Brian and H. M. McConnell, *Proc. Natl. Acad. Sci. USA*, 1984, **81**, 6159–6163.
16 P. K. W. Mary, L. Kraft, Marjorie L. Longo, Ian D. Hutcheon and Steven G. Boxer, *Science*, 2006, **313**, 1948–1951.
17 R. P. Richter and A. R. Brisson, *Biophys. J.*, 2005, **88**, 3422–3433.
18 S. Xu, G. Szymanski and J. Lipkowski, *J. Am. Chem. Soc.*, 2004, **126**, 12276–12277.
19 F. Tokumasu, A. J. Jin, G. W. Feigenson and J. A. Dvorak, *Biophys. J.*, 2003, **84**, 2609–2618.
20 W. Bücking, G. A. Urban and T. Nann, *Sensors and Actuators, B: Chemical*, 2005, **104**, 111–116.
21 A. L. Plant, M. Gueguetchkeri and W. Yap, *Biophys. J.*, 1994, **67**, 1126–1133.
22 M. B. Smith, J. Tong, J. Genzer, D. Fischer and P. K. Kilpatrick, *Langmuir*, 2006, **22**, 1919–1927.
23 M. Twardowski and R. G. Nuzzo, *Langmuir*, 2003, **19**, 9781–9791.
24 A. J. Bard and L. R. Faulkner, *Electrochemical methods: Fundamentals and Applications*, John Wiley & Sons, Inc., New York, 2001.
25 D. E. Weisshaar, M. M. Walczak and M. D. Porter, *Langmuir*, 1993, **9**, 323–329.
26 B. Zeng, X. Ding, D. Pan and F. Zhao, *Talanta*, 2003, **59**, 501–507.

27 L. Wang, J. Bai, P. Huang, H. Wang, L. Zhang and Y. Zhao, *Electrochem. Commun.*, 2006, **8**, 1035–1040.
28 D. Burshtain and D. Mandler, *Phys. Chem. Chem. Phys.*, 2006, **8**, 158–164.
29 J. T. Banks, T. T. Yu and H. Z. Yu, *J. Phys. Chem. B*, 2002, **106**, 3538–3542.
30 A. R. MacDairmid, M. C. Gallagher and J. T. Banks, *J. Phys. Chem. B*, 2003, **107**, 9789–9792.
31 R. G. Nuzzo and D. L. Allara, *J. Am. Chem. Soc.*, 1983, **105**, 4481–4483.
32 H. Wackerbarth, A. Pernille Tofteng, K. J. Jensen, I. Chorkendorff and J. Ulstrup, *Langmuir*, 2006, **22**, 6661–6667.
33 C. Vericat, M. E. Vela, G. A. Benitez, J. A. Martin Gago, X. Torrelles and R. C. Salvarezza, *J. Phys.: Condens. Matter*, 2006, **18**, R867–R900.
34 O. Azzaroni, M. E. Vela, G. Andreasen, P. Carro and R. C. Salvarezza, *J. Phys. Chem. B*, 2002, **106**, 12267–12273.
35 M. E. Vela, H. Martin, C. Vericat, G. Andreasen, A. Hernández Creus and R. C. Salvarezza, *J. Phys. Chem. B*, 2000, **104**, 11878–11882.
36 L. D. Mayer, M. J. Hope and P. R. Cullis, *Biochim. Biophys. Acta*, 1986, **858**, 161–168.
37 F. Olson, C. A. Hunt, F. C. Szoka, W. J. Vail and D. Papahadjopoulos, *Biochim Biophys Acta*, 1979, **557**, 9–23.
38 C. Love, L. A. Estroff, J. K. Kriebel, R. G. Nuzzo and G. M. Whitesides, *Chem. Rev.*, 2005, **105**, 1103–1169.
39 M. J. Esplandiu, M. L. Carot, F. P. Cometto, V. A. Macagno and E. M. Patrito, *Surface Science*, 2006, **600**, 155–172.
40 M. J. Esplandiu, H. Hagenström and D. M. Kolb, *Langmuir*, 2001, **17**, 828–838.
41 T. Y. B. Leung, M. C. Gerstenberg, D. J. Lavrich, G. Scoles, F. Schreiber and G. E. Poirier, *Langmuir*, 2000, **16**, 549–561.
42 D. G. Castner, K. Hinds and D. W. Grainger, *Langmuir*, 1996, **12**, 5083–5086.
43 C. Vericat, M. E. Vela, G. Andreasen, R. C. Salvarezza, L. Vázquez and J. A. Martín-Gago, *Langmuir*, 2001, **17**, 4919–4924.
44 C. Vericat, G. Andreasen, M. E. Vela, H. Martin and R. C. Salvarezza, *J. Chem. Phys.*, 2001, **115**, 6672–6678.
45 F. Terán Arce, M. E. Vela, R. C. Salvarezza and A. J. Arvia, *Langmuir*, 1998, **14**, 7203–7212.
46 B. A. Smith and H. M. McConnell, *Proc. Natl. Acad. Sci. USA*, 1978, **75**, 2759–2763.
47 S. G. Boxer, *Curr. Opin. Chem. Biol.*, 2000, **4**, 704–709.
48 M. Barile, C. Brizio, D. Valenti, C. De Virgilio and S. Passarella, *Eur. J. Biochem.*, 2000, **267**, 4888–4900.
49 F. Depeint, W. R. Bruce, N. Shangari, R. Mehta and P. J. O'Brien, *Chem. Biol. Interact.*, 2006, **163**, 94–112.

DOI: 10.1002/cphc.200900265

Phospholipid Bilayers Supported on Thiolate-Covered Nanostructured Gold: In Situ Raman Spectroscopy and Electrochemistry of Redox Species

M. Antonieta Daza Millone,[b] María E. Vela,[b] Roberto C. Salvarezza,[b] Tânia B. Creczynski-Pasa,[c] Nicolás G. Tognalli,*[a] and Alejandro Fainstein[a]

Thiol-covered nanostructured gold has been tested as a platform for the preparation of high-area phospholipid bilayer systems suitable for optical and electrochemical sensing. In situ and ex situ Raman spectroscopy and electrochemical measurements are made to study methylene blue (MB) and flavin-adenine dinucleotide (FAD) incorporation into dimyristoylphosphatidylcholine (DMPC) bilayers prepared by vesicle fusion on dithiothreitol (DTT)-covered nanostructured gold. Results show that lipophilic positively charged MB molecules are incorporated in the bilayer reaching the DTT-gold interface. On the other hand, the negatively charged FAD molecules are immobilized at the outer part of the phospholipid bilayer and cannot be electrochemically detected. Our results demonstrate that DTT-covered nanostructured gold provides a suitable high-area platform for phospholipid membranes that are able to separate and sense different kinds of molecules and biomolecules.

1. Introduction

Controlled design of functional biomimetic systems by self-organization has attracted considerable interest because of their wide range of potential applications that go from sensing, detection and identification devices to the development of efficient biocatalysts.[1] Also biomimetic systems are important in the field of drug carrying and drug targeting. In this context, reconstituting artificial phospholipid layers supported on solid substrates have been extensively investigated because they can be used to study, in a controlled way, basic aspects of ion, molecule and biomolecule interactions with biological materials as well as their transport across the membranes.[2,3] Phospholipid layers can also be used for exploring the interaction and transport of nanoparticles, carbon nanotubes, and other novel nanomaterials with membranes,[4] an important issue in relation to nanoscience and nanotechnological uses and concerns.

High-area solid substrates have been employed as platforms for supporting phospholipid bilayers because they provide amplification of the different signals used to detect the presence and follow the transport of species in these nanoscale environments.[5] In particular, porous nanostructured substrates are emerging as good candidates for supporting phospholipid bilayers because the membranes can retain their fluidity and they offer more interstitial free space in the pores for membrane protein incorporation or for membrane function studies. Concerning this point of view, mesoporous silicon, nanoporous ceramics and metals have been explored as promising materials. Incorporation of optically active molecular probes in membrane-covered high-area systems provides a simple way to follow structural changes under different perturbations that can be transduced into changes in optical signals.[6]

Nanostructured metals such as gold and silver are particularly interesting as platforms for supporting phospholipid bilayers because they enable the use of electrochemical[7] and optical[8] techniques. These techniques provide in situ complementary information about interaction and transport of different molecules, biomolecules or nanomaterials in self-assembled molecular layers in contact with electrolytes.[9] The study of molecule/membrane/metal interfaces immersed in aqueous environments requires the use of these substrates to take advantage of an extremely sensitive technique like surface enhanced Raman spectroscopy (SERS).[8] SERS is a very sensitive technique that employs different types of nanostructured substrates to enhance the Raman signal produced by adsorbed and immobilized species, which is otherwise too weak to be detected with conventional Raman spectroscopy.[10] Electrochemical nanostructured gold is one example of these active substrates.[11] In SERS spectroscopy, the effective Raman cross-section can be increased by many orders of magnitude. Therefore, this technique combines the ultra-sensitive detection limit with the detailed structural information content of Raman spectroscopy.[8]

[a] *Dr. N. G. Tognalli, Prof. Dr. A. Fainstein*
Laboratorio de Propiedades Ópticas
Centro Atómico Bariloche and Instituto Balseiro, CNEA
(8400) S. C. de Bariloche (Argentina)
Fax: (+54) 2944 44 5299
E-mail: tognalli@cab.cnea.gov.ar

[b] *M. A. Daza Millone, Prof. Dr. M. E. Vela, Prof. Dr. R. C. Salvarezza*
Laboratorio de Nanoscopías y Fisicoquímica de Superficies
INIFTA, CONICET-UNLP
CC16 Suc. 4 (1900) La Plata (Argentina)

[c] *Prof. Dr. T. B. Creczynski-Pasa*
Departamento de Ciências Farmacêuticas
Universidade Federal de Santa Catarina, UFSC
C. P. 476 (88.040-900) Florianópolis (Brazil)

Vesicles of phospholipids can adsorb on thiol-covered polycrystalline gold.[12] Thiol monolayers terminated with hydrophilic functional groups such as alcohols promote the adsorption and rupture of vesicles to generate patches of bilayers supported by the underlying thiol layer. On the other hand, hydrophobic methyl-terminated thiols promote the formation of hybrid bilayers formed by the thiol monolayer and a single layer of phospholipids.[12]

Recently, we have prepared fluid dimyristoylphosphatidylcholine (DMPC) bilayers on dithiothreitol (DTT) covered Au(111) by vesicle fusion.[13] The OH-rich DTT monolayer turns the Au surface hydrophilic enough to allow vesicle fusion[14] as revealed by in situ atomic force imaging. Methylene blue (MB) and flavin adenine dinucleotide (FAD) have been used as probes to study molecule transport across the bilayer. The possibility of DMPC bilayer formation on DTT-covered nanostructured Au is very attractive because it opens the possibility of increasing the electrical signal for amperometric detection and also allows the use of optical detection by SERS. However, some questions should be answered: Is it possible to form continuous membranes on these disordered structures that have high density of nanocolumns and nanopores? Is the high area, which practically fills the volume of the nanostructured layer, accessible to analytes? Is it possible to study the electrochemical and optical response of molecules confined in the bilayer?

Herein we have used dithiothreitol (DTT)-covered nanostructured gold as a solid platform for phospholipid bilayer formation. We have used in situ Raman and electrochemical data to follow in real time the behavior of MB and FAD immobilized in the bilayer. In situ SERS data show that MB incorporates in the DMPC bilayer and diffuses to reach the DTT-gold surface. On the other hand, FAD remains in the outer part of the bilayer far from the DTT-gold surface being, then, electrochemically inactive. In addition, we observe FAD expelling from the bilayer to the electrolyte when the gold surface becomes negative. This seems to be related to subtle changes in the gold-phospholipid bilayer-FAD interactions induced by the applied potential. Therefore, phospholipids bilayers supported in high area nanostructured gold appear as promising systems to sense and to separate lipophilic and lipophobic species in a simple way. This can be also used as a biomimetic system to study the physical chemistry of methylene blue, or other drugs investigated as candidates for photodynamic therapy, confined in phospholipid membranes.[2]

2. Results and Discussion

2.1. DMPC-DTT-Au: Selective Electrochemical Detection

First, we have studied the ability of the DMPC-DTT-Au system for selective electrochemical detection/separation of mixtures of redox molecules in solution according to their lipophilic properties. This experiment enables to test the bilayer continuity because we expect that for a continuous system a negatively charged molecule as FAD should not reach the Au surface. Meanwhile MB should be able to diffuse across the bilayer due to its lipophilic nature. Note that in this experiment, as FAD and MB molecules form part of the electrolytic solution, a concentration gradient could induce permeation of molecules across non-covered patches or defects reaching the Au surface where they could be electrochemically detected. For this purpose DMPC-DTT-Au either on smooth or nanostructured electrodes were immersed in mixed solutions containing 5×10^{-6} M MB + 10^{-5} M FAD in 0.1 M phosphate buffer pH 7.4 solution, and cyclic voltammograms were recorded (Figures 1 a,b). We

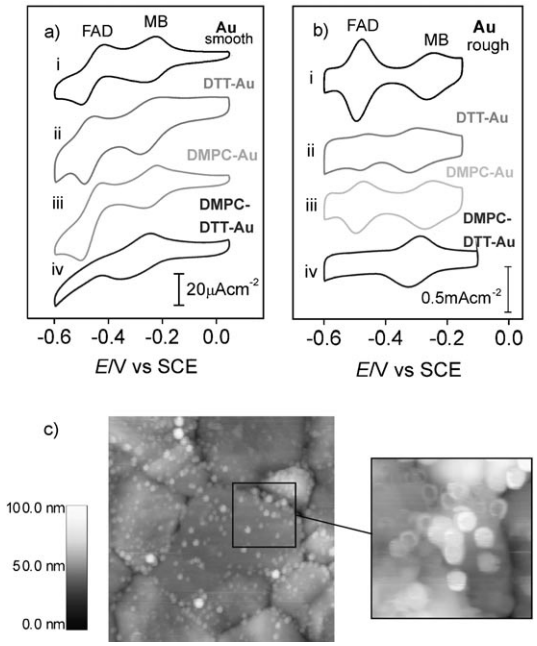

Figure 1. Cyclic voltammograms performed in 5×10^{-6} MB + 10^{-5} M FAD in 0.1 M phosphate buffer pH 7.4 at 25 °C for: a) smooth gold: (i) bare Au, (ii) DTT-Au, (iii) DMPC-Au and (iv) DMPC-DTT-Au at a scan rate of 0.20 V s^{-1} and for b) nanostructured (rough) gold: (i) bare Au, (ii) DTT-Au, (iii) DMPC-Au and (iv) DMPC-DTT-Au at a scan rate of 0.10 V s^{-1}.Current density is referred to the geometric area of each gold electrode. c) 5 μm × 5 μm in situ contact AFM image of the DMPC-Au surface (*Z* height = 100 nm). Intact DMPC vesicles and clean gold areas are clearly observed. Inset: 1.5 μm × 1.5 μm AFM image of vesicles (*Z* height = 40 nm).

have also included bare Au, DTT -Au and DMPC -Au substrates as blank experiments. For the bare Au, DTT-Au and DMPC-Au electrodes (smooth and nanostructured) both redox couples are clearly observed (Figures 1 a,b i–iii). In contrast for DMPC-DTT-Au surfaces (Figures 1 a,b iv) only the MB redox couple is electrochemically detected indicating that the FAD molecules have no access to the DTT-Au interface in order to participate in the charge-transfer process due to the presence of the DMPC bilayer. Also, the fact that the FAD redox couple is not inhibited on the DMPC-Au substrate (Figures 1 a,b iii) demonstrates the key role of the DTT monolayer to form a continuous bilayer by providing a hydrophilic surface for the vesicle fusion. In fact, in situ AFM images of the DMPC-Au (smooth substrate) show intact vesicles on the substrate (Figure 1 c) indicating that the continuous bilayer is not formed on the bare Au under our experimental conditions. Note that the vesicles

are constituted by a soft material and the tip causes a typical concave deformation (Figure 1 c, inset) as already reported.[15]

Therefore, we can conclude that in both substrates the phospholipid bilayer is continuously hindering FAD penetration and allowing only the permeation of the lipophilic MB molecules. However, it is important to note that there is a large increase (about 25 times) in the current related to the MB redox couple in the DMPC-DTT-nanostructured Au compared to that measured for DMPC-DTT-Au(111) surface, that is, the high-area nanostructured substrate can detect smaller amount of molecules in the solution.

2.2. In Situ Raman Electrochemistry

In this section we will show results for combined optical and electrochemical detection of very small amounts of molecules trapped/confined in the phospholipid bilayer. As has been previously studied by Tognalli et al.,[16] submonolayer amounts of MB can be immobilized in alkanethiolate self-assembled monolayers on nanostructured Au and detected by combined electrochemistry and SERS. However, hydrophobic and hydrophilic thiols trap MB with different efficiency and at different locations of the SAM.[16] DMPC bilayers supported on DTT SAM have both hydrophilic and hydrophobic moieties, therefore MB interaction with this phospholipid bilayer system must be first analyzed.

Supported DMPC bilayers exhibit no well defined signals in their spectra (Figure 2, bottom). Meanwhile, we observe the characteristic vibrational modes coming from FAD and MB

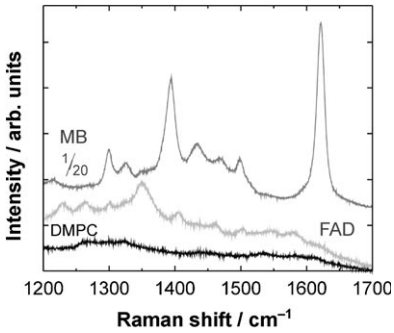

Figure 2. SERS spectra recorded for MB (top) and FAD (middle) immobilized in DMPC supported on DTT-covered nanostructured gold. Samples were taken in air (dried samples) with the 647.1 nm laser line. The MB intensity was divided 20 times to fit in the figure. The SERS spectra of the DMPC-DTT substrate (bottom) was also collected as a blank experiment.

when they are immobilized in DMPC supported on DTT modified gold electrodes.[17-19] The MB and FAD immobilization were performed through a 30 min incubation at 37 °C in their respective solutions. The difference in the intensity of the Raman signals between the MB and FAD spectra reflects the much larger electronic resonant enhancement of MB, as compared to FAD, for laser excitation at 647.1 nm.

In Figure 3 we present SERS spectra taken with the 568.1 nm laser line recorded for MB in DMPC supported on DTT-covered

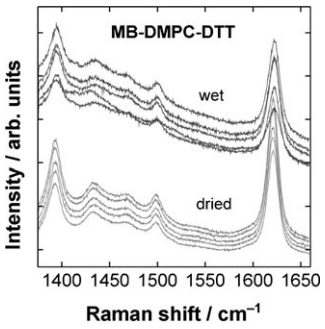

Figure 3. SERS spectra recorded for MB in DMPC supported on DTT-covered nanostructured gold taken in air (dried, lower) and in phosphate buffer at open circuit potential (ocp) (wet, upper). The spectra were taken with 568.1 nm laser excitation. Each spectrum was taken at a different place of the sample to show the homogenous behavior of the system.

nanostructured gold taken in air (dried) and in phosphate buffer at open circuit potential (ocp) (wet), that is, without polarization of the gold electrode. In both cases we observe the typical Raman spectra already reported for MB bonded to S and alkanethiolate self-assembled monolayers on gold surfaces.[16] The spontaneous potential reached by the system (the ocp) is −0.2 V so that the MB molecule is in the oxidized state as MB^+. We note from these spectra that simple immersion of the DMPC containing MB molecules in the electrolyte solution results in a 25% decrease in the signal intensity suggesting that MB^+ species can partially diffuse from the phospholipid bilayer to the electrolyte. Therefore, we conclude that this signal loss is related with "free" MB species in the DMPC bilayer.

SERS spectra in Figure 4 were acquired as a function of the applied potential during the first cyclic voltammogram in a 0.1 M phosphate buffer pH 7.4 at 20 °C for the "trapped" MB molecules, that is, those MB molecules that remain in the DMPC membrane after immersion. The potential was scanned from 0 to −0.5 V, and back to −0.1 V, so that MB evolves from its natural oxidized state, to being fully reduced, and finally back again to its oxidized form.

The scan rate employed was 0.01 $V s^{-1}$, the Raman acquisition was 1 s and spectra were taken every 2 s. So each Raman

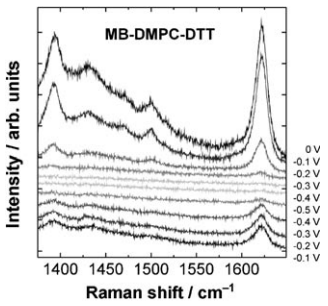

Figure 4. SERS spectra recorded for MB immobilized in DMPC supported on DTT-covered nanostructured gold in phosphate buffer 0,1 M pH 7.4 at 20 °C as function of the applied potential during the first cyclic voltammogram. The spectra were taken with 568.1 nm laser excitation and potentials are referred to Ag/AgCl electrode.

spectrum is the MB response at each specified potential. The scan rate and Raman acquisition time chosen were the best condition found as a compromise to avoid both MB diffusion to the solution and photobleaching, and registering Raman spectra with a good signal to noise ratio.

It is observed that the intensity of the peaks undergoes important changes as a function of the applied potential while the overall shape of the Raman spectra is conserved along the electrochemical run. The most important feature in the spectra is the marked decrease in the intensity that becomes null when the potential reaches −0.5 V. At this potential all MB^+ molecules are transformed in MBH (reduced) species that are not electronic resonant for yellow (568.1 nm) excitation.

However, when the potential returns to −0.1 V the intensity of the SERS signals does not recover its initial value. In fact, only about 20% of the original signal arising from the MB^+ species is observed after the first complete scan. Note that we have not observed substantial photobleaching either at ocp or in Raman measurements performed in situ during cyclic voltammograms performed on MB immobilized on different thiol SAMs and with similar integration times.[9] This indicates that a large number of molecules immobilized in the DMPC membrane diffuse to the solution during the first potential cycle. In contrast to the spontaneous diffusion of free MB^+ species observed at ocp this diffusion process is induced by the applied potential. In fact, it is well known that the leuco MBH species exhibit a weak interaction with the hydrocarbon chains, thus being free to diffuse to the electrolyte. After the rapid decay observed in the first voltammetric run the signal intensity decays only to 75% in the following potential cycles. Another interesting fact is that practically all the remaining MB molecules are electrochemically active since no background signal (as would be expected for MB molecules that remain in the oxidized state) is observed when the potential reaches −0.5 V.

Now we discuss the behaviour of FAD molecules. SERS spectra in Figure 5 were taken in air for bare and DMPC-DTT nanostructured gold substrates after incubation with FAD solution (see Experimental Section). All peaks (except the one indicated with an asterisk which originates from a plasma line) shown in the spectra at ocp can be identified with FAD vibrations.[17] It becomes evident from the upper curve of Figure 5 that oxidized FAD molecules are present in the bilayer after the incubation when the supported bilayer-gold surface is at its open circuit potential. It follows from Figure 5 that we observe similar SERS intensities for FAD-Au as compared to FAD immobilized in the bilayer. However, we know that SERS amplification depends on the distance to the substrate,[16] and no FAD redox couple have been observed in the DMPC supported system (Figure 1). These results could imply either the presence of a larger amount of FAD in the phospholipid bilayer modified substrate, or in addition some penetration of the molecules in the outer part of the bilayers that are far enough to participate in charge-transfer processes. In any case, from the SERS data in Figure 5 we can conclude that FAD is immobilized on the DMPC-DTT-gold system at least as efficiently as on the nanostructured gold without the bilayer.

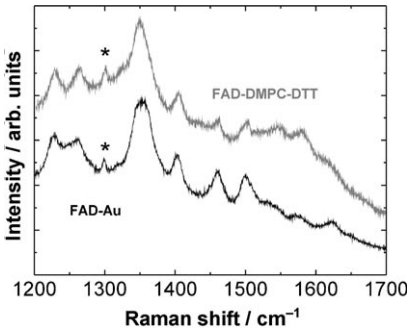

Figure 5. SERS spectra recorded for FAD immobilized in DMPC supported on DTT-covered nanostructured gold and bare nanostructured gold. The spectra were taken in air (dried samples) with 647.1 nm laser excitation. The peaks indicated with asterisks originate from a plasma line.

We have taken in situ SERS spectra in phosphate buffer at ocp and at different applied potentials after immobilization of FAD molecules in the DMPC bilayer. The spectra recorded at ocp (Figure 6) clearly demonstrate that oxidized FAD molecules

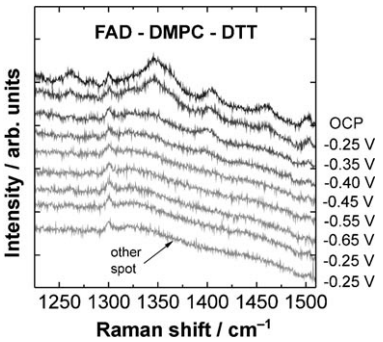

Figure 6. SERS spectra recorded for FAD immobilized in DMPC supported on DTT-covered nanostructured gold in phosphate buffer 0,1 M pH 7.4 at 20 °C as function of the applied potential during the first cyclic voltammogram. The spectra were taken with 647.1 nm laser excitation and potentials are referred to Ag/AgCl electrode.

are present in the bilayer after immersion in buffer solution as all peaks measured in the dry sample (Figure 5) are present. Again for the FAD molecules we observe that SERS intensity diminishes when the bilayer is immersed in the electrolyte but in this case is about 1/3 of the initial value, which is more pronounced than for the MB molecule. This decrease is related to a release of FAD molecules weakly bound to the external interface of the DMPC bilayer which are highly exposed to the electrolyte and diffuse due to the concentration gradient.

Results also indicate that when the applied potential becomes more negative than −0.25 V the SERS signals decrease, and finally they completely disappear at −0.45 V. It is interesting to note that, in contrast to MB, reduced FAD species should exhibit a resonant Raman amplification at 647.1 nm,[17] which in this case was not observed. Furthermore, reversing the potential in the anodic direction to −0.10 V does not result in the recovery of the signals intensity. Therefore, all these data indicate that FAD molecules have been eliminated from the bilayer. A possible explanation for this behaviour is

that these spectra were recorded at a very slow scan rate (0.05 V steps waiting 10 min at each potential value) so that there is enough time for the weakly bound FAD molecules to diffuse to the bulk solution. Another reason is related to the applied potential that induces subtle changes in the bilayer[20–23] resulting in FAD desorption. However, we observe a similar behaviour for FAD directly immobilized either on DTT SAM or bare gold, that is, without DMPC bilayer. In this case desorption of the negatively charged FAD takes place because the applied potential of the Au surface becomes more negative than the zero charge potential.[24] Indeed, it is well known that anion desorption from the Au surfaces takes place when the potentials are more negative than the zero charge potential of gold.

From the above results we can infer that the isoalloxazine moiety of the FAD molecule could be partially incorporated in the outer phospholipids layer since it is structurally similar to the MB molecule. Meanwhile, the hydrophilic negatively charged moiety of FAD remains in contact with the electrolyte (Figure 7). On the other hand, MB molecules are incorporated

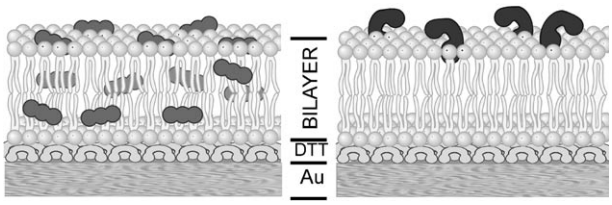

Figure 7. Proposed scheme for the location of MB (left) and FAD (right) molecules in the DMPC-DTT-Au system. The molecules in the outer plane of the bilayer are lost after immersion.

in the overall DMPC bilayer volume but only those located closer to the gold surface are electrochemically active (Figure 7). The rest of the molecules are more easily released to the electrolyte, first upon immersion and afterwards by electrochemical cycling as reduced MBH molecules are formed. If one considers that the permeability of MB through a phospholipid bilayer is about 10^{-9} cm s^{-1}–10^{-10} cm s^{-1}[25] and the scan rate in the SERS measurements is 0.010 V s^{-1}, we can identify the confined MB with those molecules closer to the DTT-gold surface. These molecules have no time to diffuse as MBH from this interface across the membrane to the electrolyte before they are reoxidized to MB^+.[16]

Therefore, we can assume that the bilayer structure is similar on both the smooth and nanostructured substrates because the transport properties of the molecules are quite similar.

Advantages of nanostructured gold as a platform for sensing devices are evident: the electrical signal is more than one order of magnitude larger on these substrates, they exhibit SERS activity for optical detection and they act as a spongy-like material where lipophilic molecules can be preconcentrated thus improving the detection limit. Finally, recent XPS data show that the rate of thiol oxidation on nanostructured Au is smaller than in planar Au,[26] entailing that the stability of the overall system can also be improved by the use of rough substrates.

3. Conclusions

- DTT-covered nanostructured gold can be used to prepare phospholipid bilayers. The DTT SAM allows charge transfer turning the system suitable for electrochemical sensing.
- We test the quality of the DMPC bilayer for optical and electrochemical sensing using the positively charged lipophilic MB and the negatively charged lipophobic FAD.
- Our results demonstrate that MB molecules easily penetrate the phospholipids bilayer diffusing to the DTT-gold interface where they are detected by voltammetry. In contrast, FAD molecules remain immobilized at the outer part of the bilayer. They are expelled to the electrolyte as the gold surface becomes negative.
- Three different behaviours can be observed for MB: 1) free MB species, that diffuse to the electrolyte in the absence of MB in solution, 2) MB molecules that are removed from the phospholipid bilayer only when they are reduced to the leuco MBH species, 3) MB molecules that remain confined in the bilayer.
- DTT-covered nanostructured gold provides a suitable high area platform for phospholipid bilayers. The DMPC-DTT-nanostructured gold separate lipophilic from lipophobic molecules allowing their detection by electrochemical and optical method.

Experimental Section

We have performed experiments with dimyristoylphosphatidylcholine (DMPC) bilayers supported on dithiothreitol (DTT)-covered gold substrates and we test them against a mixed solution of MB and FAD. In addition, both molecules were separately immobilized in order to understand its interaction with the DMPC bilayer.

Substrate Preparation: Two different types of Au substrates were used. 1) Smooth gold: Polycrystalline gold films (250 nm in thickness) were prepared by physical vapor deposition on a 4 nm chromium layer on glass (Gold Arrandee™). A three minute flame annealing was performed to generate micrometer sized crystals separated by deep grain boundaries. Software analysis of 5 μm × 5 μm images gives a root mean square (RMS) roughness of ~12 nm. The micrometer sized crystals exhibit atomically smooth Au(111) terraces, separated by monoatomic steps[27] (Figure 8a). 2) Nanostructured gold (Figure 8b): SERS active nanostructured gold was prepared by the electrochemical roughening procedure described in ref. [11]. Briefly, a thick hydrous Au oxide film is formed by anodization of Au at a relatively high applied potential followed by voltammetric electroreduction. Au foils 99.99% purity were used, that were immersed in a 0.5 M H_2SO_4 solution and held for 15 min at 2.4 V (vs SCE as reference electrode). Finally, the potential was scanned down to −0.6 V at a rate of 0.025 V s^{-1}. The surface of the resulting electrodes consists of 10 to 20 nm Au nanosized grains while the thickness reaches 650–1000 nm.[28] The RMS measured by STM is relatively low (~85 nm in 5 μm × 5 μm images) because the tip cannot penetrate the nanometer sized pores between the small crystals. The real surface area of these high area electrodes was calculated by measuring the AuO monolayer electroreduction charge

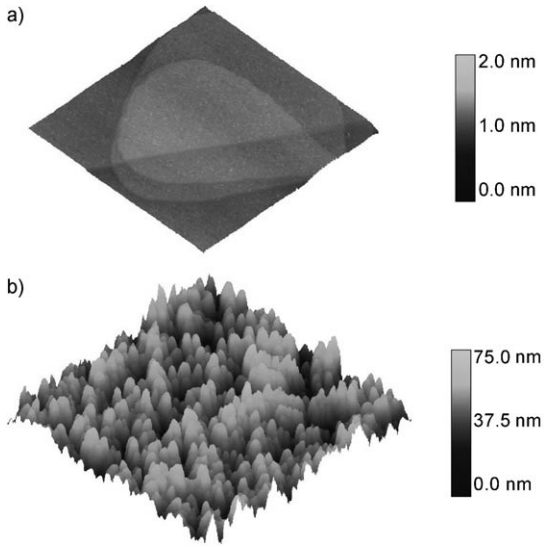

Figure 8. STM images in air of smooth (a) and nanostructured (b) gold, scan size: 600 nm × 600 nm.

(q),[11] considering that one monolayer involves 0.42 mC cm^{-2}. Values of real surface area used in this work were in the 25–35 cm^2 range.

STM measurements of these substrates were carried out with a Nanoscope IIIa (Veeco, Santa Barbara, USA) using Pt/Ir tips. Typical measurements conditions were 0.2 V of bias potential and 1 nA of current setpoint.

Chemicals: DL-Dithiothreitol (DTT), 4-(2-hydroxyethyl)-1-piperazineethanesulphonic acid (HEPES) and flavin adenine dinucleotide (FAD) were purchased from Sigma, dimyristoylphosphatidylcholine (DMPC) was purchased from Avanti and methylene blue (MB) from Merck. All other supplies used were of the best analytical grade commercially available.

DTT-Self Assembly on Gold Substrates: The DTT SAMs were prepared by immersion of the gold substrates in 50 μM DTT ethanolic solution at 60 °C for 30 min. XPS and electrochemical data have shown that the DTT SAM consists of a close packed array of lying down molecules exposing the OH groups to the solution.[13] The lying down DTT molecules on the gold substrates provides the hydrophilic environment able to promote the vesicle fusion to form the phospholipid bilayer.

Self-assembly of Phospholipidic Bilayers on DTT-Covered Gold Substrates: DMPC vesicles were obtained by evaporating, under a stream of nitrogen, the solvent of a phospholipidic solution (10 mg mL^{-1}) prepared in chloroform.[13] To eliminate possible traces of the solvent, the samples were dried under vacuum. Subsequently, multilamellar vesicles were obtained by the addition of a buffer containing 10 mM HEPES + 0.9% NaCl and vortexing. The multilamellar suspension was then extruded through a polycarbonate filter with 400 nm pore from Nuclepore to form unilamellar vesicles.[29,30] The DMPC bilayers were prepared by vesicle fusion on the DTT-covered gold by immersing the substrates in 10 mg mL^{-1} DMPC vesicle suspension for 90 min at ~30 °C (above DMPC phase transition temperature).

Blank experiments using Au without DTT were also made. AFM measurements were performed at pH 7.4 with a Molecular Imaging PicoScan microscope inside a fluid cell with temperature control, that is, in situ, containing 10 mM HEPES + 0.9% NaCl, under contact mode with silicon nitride probes (triangular cantilevers with nominal spring constant of 0.12 N m^{-1}, Veeco Probes). The images were analyzed using the program WSxM 5.0 (Nanotec Electronica).[31]

Immobilization of Redox Biomolecules: DMPC supported bilayers on the DTT-covered Au substrates were dipped in 0.1 mM methylene blue (MB) or 0.1 mM flavin adenine dinucleotide (FAD) aqueous solutions for 30 min at 37 °C, a temperature where the phospholipidic bilayer is in a fluid phase. The samples were then carefully rinsed with water, dried under nitrogen flux and used for Raman and electrochemical measurements. Blank experiments using DTT-covered Au substrates were also made.

Raman Measurements: The Raman experiments were made in situ using a Jobin–Yvon T64000 triple spectrometer operating in subtractive mode and equipped with a liquid-N_2 cooled charge coupled device. The excitation was done with an Ar-Kr ion laser using energies between 1.834 eV (676 nm) and 2.707 eV (458 nm). Typical powers were around 10 mW, concentrated on a 7 mm long and ~100 μm wide line focus. This was chosen to reduce the photon induced degradation of the samples. The photobleaching was determined to be less than 5% after 100 s of data acquisition. To avoid accumulating this effect, a fresh spot in the sample was used after taking each spectrum. Prior to this a Raman map of the samples was performed with very low powers and acquisition time to exclude spots displaying Raman intensities very different from the average value. To check for repeatability, five complete series of measurements were performed.

Electrochemical Measurements: Experiments with the redox couples were performed in a conventional electrochemical cell using a large platinum plate as counter electrode and saturated calomel as reference electrode (SCE), using a TEQ-2 potentiostat with data acquisition capability. Phosphate buffer 0.1 M pH 7.4 was used as electrolyte and it was bubbled during 2 h with purified nitrogen to remove oxygen.
For the experiments with redox couples in a mixed solution, 5×10^{-6} MB + 10^{-5} M FAD in phosphate buffer 0.1 M pH 7.4 were employed. Measurements made with nanostructured gold required 15 min of preconcentration in the mixed solution before performing the electrochemical experiments due to different diffusion paths in nano/microcavities with respect to smooth gold.

Acknowledgements

We acknowledge financial support from ANPCyT (PICT 06-621), CONICET (PIP 6075) and CNPq/Prosul. This paper was made in the frame of the Interfacial, Supramolecular and Molecular Nanoscience and Nanotechnology Net (PAE 22711) and Nanoscience and Nanotechnology Net: Nanostructured Materials and Systems (Argentina). M.E.V. is a member of the research career of CIC.

Keywords: electrochemistry · dinucleotides · methylene blue · SERS · phospholipid

[1] C. Sanchez, H. Arribart, M. M. G. Guille, *Nat. Mater.* **2005**, *4*, 277–288.
[2] E. Sackmann, *Science* **1996**, *271*, 43–48.
[3] K. Tawa, K. Morigaki, *Biophys. J.* **2005**, *89*, 2750–2758.
[4] S. K. Banerji, M. A. Hayes, *Langmuir* **2007**, *23*, 3305–3313.
[5] F. Cunin, P. E. Milhiet, E. Anglin, M. J. Sailor, C. Espenel, C. Le Grimellec, D. Brunel, J. M. Devoisselle, *Ultramicroscopy* **2007**, *107*, 1048–1052.

[6] M. K. Park, A. V. Tepikin, O. H. Petersen, *Pfluegers Arch.* **2002**, *444*, 305–316.
[7] R. C. Salvarezza, A. J. Arvia in *Modern Aspects of Electrochemistry* (Eds.: B. E. Conway, J. O. M. Bockris, R. E. White), Plenum, New York, **1996**, pp. 289–373.
[8] M. Moskovits, *J. Raman Spectrosc.* **2005**, *36*, 485–496.
[9] N. G. Tognalli, A. Fainstein, C. Vericat, M. E. Vela, R. C. Salvarezza, *J. Phys. Chem. C* **2008**, *112*, 3741–3746.
[10] K. Kneipp, H. Kneipp, I. Itzkan, R. R. Dasari, M. S. Feld, *J. Phys. Condens. Matter* **2002**, *14*, R597–R624.
[11] C. Vericat, G. A. Benitez, M. E. Vela, R. C. Salvarezza, N. G. Tognalli, A. Fainstein, *Langmuir* **2007**, *23*, 1152–1159.
[12] C. Love, L. A. Estroff, J. K. Kriebel, R. G. Nuzzo, G. M. Whitesides, *Chem. Rev.* **2005**, *105*, 1103–1169.
[13] T. B. Creczynski-Pasa, M. A. Daza Millone, M. L. Munford, V. R. d. Lima, T. O. Vieira, G. A. Benitez, A. A. Pasa, R. C. Salvarezza, M. E. Vela, *Phys. Chem. Chem. Phys.* **2009**, *11*, 1077–1084.
[14] W. Caetano, P. S. Haddad, R. Itri, D. Severino, V. C. Vieira, M. S. Baptista, A. P. Schroder, C. M. Marques, *Langmuir* **2007**, *23*, 1307–1314.
[15] G. Mao, X. Liang, K. Y. S. Ng, *Dekker Encyclopedia of Nanoscience and Nanotechnology*, Marcel Decker, New York, **2004**, pp. 932–942.
[16] N. G. Tognalli, A. Fainstein, C. Vericat, M. E. Vela, R. C. Salvarezza, *J. Phys. Chem. B* **2006**, *110*, 354–360.
[17] W. D. Bowman, T. G. Spiro, *Biochemistry* **1981**, *20*, 3313–3318.
[18] K. Hutchinson, R. E. Hester, W. J. Albery, A. R. Hillman, *J. Chem. Soc. Faraday Trans. 1* **1984**, 2053–2071.
[19] R. R. Naujok, R. V. Duevel, R. M. Corn, *Langmuir* **1993**, *9*, 1771–1774.
[20] T. C. Anglin, J. C. Conboy, *Biophys. J.* **2008**, *95*, 186–193.
[21] I. Burgess, M. Li, S. L. Horswell, G. Szymanski, J. Lipkowski, J. Majewski, S. Satija, *Biophys. J.* **2004**, *86*, 1763–1776.
[22] L. J. Jeuken, *Biophys. J.* **2008**, *94*, 4711–4717.
[23] E. A. Disalvo, F. Lairion, F. Martini, E. Tymczyszyn, M. Frias, H. Almaleck, G. J. Gordillo, *Biochim. Biophys. Acta* **2008**, *1778*, 2655–2670.
[24] A. Hamelin in *Modern Aspects of Electrochemistry, Vol. 16* (Eds.: B. E. Conway, R. E. White, J. O. M. Bockris), Plenum, New York, **1985**, p. 30.
[25] A. L. Zanocco, G. Günther, E. Lemp, E. A. Lissi, *J. Chem. Soc. Perkin Trans. 1* **1998**, *2*, 319–324.
[26] C. Vericat, M. E. Vela, G. A. Benitez, J. A. Martin Gago, X. Torrelles, R. C. Salvarezza, *J. Phys. Condens. Matter* **2006**, *18*, R867–R900.
[27] G. Andreasen, M. E. Vela, R. C. Salvarezza, A. J. Arvia, *Langmuir* **1997**, *13*, 6814–6819.
[28] P. Herrasti, P. Ocón, R. C. Salvarezza, J. M. Vara, L. Vázquez, A. J. Arvia, *Electrochim. Acta* **1992**, *37*, 2209–2214.
[29] L. D. Mayer, M. J. Hope, P. R. Cullis, *Biochim. Biophys. Acta Biomembr.* **1986**, *858*, 161–168.
[30] F. Olson, C. A. Hunt, F. C. Szoka, W. J. Vail, D. Papahadjopoulos, *Biochim. Biophys. Acta Biomembr.* **1979**, *557*, 9–23.
[31] I. Horcas, R. Fernandez, J. M. Gomez-Rodriguez, J. Colchero, J. Gomez-Herrero, A. M. Baro, *Rev. Sci. Instrum.* **2007**, *78*, 013705.

Received: April 3, 2009
Revised: May 16, 2009
Published online on July 13, 2009

Lista de ilustraciones de los capítulos